snowpex

SnowPEx –

The Satellite Snow Product Intercomparison and Evaluation Exercise

Guidelines for the Generation of Snow Extent Products from High Resolution Optical Sensors – FINAL

Deliverable D8

Prepared by

Elisabeth Ripper, Gabriele Schwaizer, and Thomas Nagler, ENVEO, Austria

Sari Metsämäki and Markus Törmä, Finnish Environment Institute, SYKE, Finland

Richard Fernandes, CCRS, Canada

Christopher J. Crawford, NASA/GSFC, USA

Thomas Painter, JPL, USA

Karl Rittger, NSIDC, USA

Issue / Revision: 2 / 1

Date: 17.04.2019

Document controlled by: Gabriele Schwaizer

SnowPEx Report

SUBJECT:	**PROJECT COORDINATOR:**
Guidelines for the generation of snow extent products from high resolution optical sensors – FINAL	ENVEO

ISSUE / REVISION:	CONTRACTOR'S REF:
2 / 1	Deliverable D8

This deliverable provides the final version of the description of the methods for generation of snow maps from Landsat data intended for evaluation of medium resolution hemispheric / global snow extent products. The processing steps including topographic correction, various snow detection algorithms, and cloud screening. Further, the method applied for aggregation from Landsat pixel spacing to lower resolution is described. An overview on the Landsat scenes used within SnowPEx is also given. A detailed description of the Landsat data sets is provided in Deliverable 9.

This updated document version includes information on adaptations of algorithms and processing lines for snow map generation from Sentinel-2 data.

This project was funded by the European Space Agency. Responsibility for the contents resides is the author or organisation that prepared it.

AUTHORS:
E. RIPPER, G. SCHWAIZER, T. NAGLER (ENVEO); R. FERNANDES (CCRS); S. METSÄMÄKI (SYKE); M. TÖRMÄ (SYKE); C.J. CRAWFORD (NASA); T. PAINTER (JPL); K. RITTGER (NSIDC)

This page is intentionally left blank.

DOCUMENT CHANGE LOG

Issue/ Revision	Date	Modification	Author	Observations
0/1	13.10.2015	Document created, general updates	Gabriele Bippus	Document created (adopted from SnowPEx Del-5 1/0)
0/2	13.10.2015	Document updated	Gabriele Bippus, input from Karl Rittger	Update of TMSCAG description, refinements from ISSPI-2 workshop included
0/3	14.10.2015	Updates and corrections	Elisabeth Ripper, Gabriele Bippus	
0/4	14.10.2015	Acceptance of corrections, document formatted	Gabriele Bippus	
1/0	14.10.2015	Final Version	Gabriele Bippus	
1/1	17.3.2016	Additions of Chapter 3.4	Markus Törmä	Update of auxiliary data
1/2	19.3.2016	Addition of Chapter 6.3.5	Sari Metsämäki	Documentation of SCAmod for high resolution SE map generation
1/3	07.03.2016	Updated document regarding CCN	Elisabeth Ripper	Documentation for Sentinel-2 added
1/4	31.03.2016	Compilation of contributions	Gabriele Bippus	Harmonization and check / revision of contributions 1/1 – 1/3
1/5	01.04.2016	Check and revision of full document	Gabriele Bippus	Major corrections and revisions in the document
2/0	01.04.2016	Final updated Version	Gabriele Bippus	Final check and formatting
2/1	17.04.2019	Correction of eq. 5.5	Gabriele Schwaizer	

This page is intentionally left blank.

TABLE OF CONTENTS

1. INTRODUCTION 1

1.1 Purpose 1
1.2 Structure of the Document 1
1.3 Acronyms 1

2. LANDSAT DATASET FOR SNOWPEX 5

3. AUXILIARY DATA 7

3.1 Digital Elevation Model 7
3.2 Surface Classification Maps (SCM) 7
3.3 Canopy Closure / Crown Coverage in Landsat 8 OLI / Sentinel-2 MSI resolution 8

4. OVERVIEW OF GENERATION OF LANDSAT SNOW REFERENCE DATA SET 11

5. PRE-PROCESSING OF LANDSAT DATA 13

5.1 Landsat Data Specifications 13
5.2 Orthorectification 14
5.3 Pixel Reference and Size 15
5.4 Radiometric Calibration 15
5.5 Topographic Correction 17
5.6 Cloud Detection 18

6. SNOW MAP GENERATION FROM LANDSAT DATA 21

6.1 Snow Map Coding 21
6.2 Common Pre-Processing Steps 22
6.3 Landsat Snow Mapping Algorithms 23

7. RESAMPLING METHOD OF HIGH RESOLUTION SNOW MAPS 27

8. LANDSAT OUTPUT LAYERS 28

8.1 High Resolution Maps 29

8.2 Medium/Low Resolution Maps 29

9. QUALITY ASSESSMENT OF LANDSAT SNOW MAPS 31

9.1 Method 31

9.2 Intercomparison of Landsat Snow Algorithms 31

10. DEVELOPMENT OF NEW METHODS FOR HIGH RESOLUTION SNOW MAPS FROM LANDSAT OR SENTINEL-2 35

10.1 Test data 36

10.2 Snow map generation in mountainous terrain 37

10.3 Snow map generation in boreal forested areas 42

11. REFERENCES 49

1. INTRODUCTION

1.1 Purpose

The purpose of this document is to describe a common processing concept for the preparation of high resolution snow maps from Landsat and Sentinel-2 for quality assessment of hemispheric medium resolution snow extent products. The aim is to provide a transparent description of the processing line for the high resolution snow maps to the community.

1.2 Structure of the Document

This document is split into 9 chapters. Chapter 1 provides a brief introduction to Landsat snow cover mapping, followed by chapter 2 showing the Landsat reference data set. Chapter 0 introduces the auxiliary data, such as the applied digital elevation models and surface classification. Chapter 4 shows the general concept for preparing snow maps from Landsat data. The preparation steps performed before applying Landsat snow retrieval algorithms are documented in Chapter 5, including radiometric calibration and topographic correction. Chapter 0 describes the snow algorithms to obtain binary or fractional snow maps from Landsat imagery, followed by the resampling method of Landsat high resolution snow maps to lower resolution snow maps in Chapter 7. Within chapter 0 the final products layers are listed. Chapter 9 gives a quality assessment of the Landsat snow maps derived by different algorithms. In Chapter 10 the development of a new algorithms for snow maps from Landsat or Sentinel-2 in mountainous and boreal forested areas are described. Chapter 11 lists the references mentioned in the document.

1.3 Acronyms

ACCA.SEAS	Automatic Cloud Cover Assessment, seasonal
ASTER	Advanced Spaceborne Thermal Emission and Reflection Radiometer
ASTER GDEM2	ASTER Global Digital Elevation Model Version 2
AUX	Auxiliary
BIN	Binary Snow Extent
CC	Crown Coverage
CDED	Canadian Digital Elevation Data
DEM	Digital Elevation Model
DN	Digital Number
ENVEO	Environmental Earth Observation IT GmbH

ESA	European Space Agency
ESRI	Environmental Systems Research Institute
ETM+	Enhanced Thematic Mapper Plus
EU-DEM	Digital Elevation Model for European Union countries
FSC	Fractional Snow Cover
FTP	File Transfer Protocol
HR	High Resolution
HRL	High Resolution Layer
JPL	Jet Propulsion Laboratory
LR	Low Resolution
LS-8	Landsat 8
MR	Medium Resolution
MSI	Multispectral Imager
NASA	National Aeronautics and Space Administration
NDSI	Normalized Difference Snow Index
NED	National Elevation Dataset over United States
NDSI	Normalized Difference Snow Index
NDVI	Normalized Difference Vegetation Index
NFI	National Forest Inventory
NSIDC	National Snow and Ice Data Center
OLI	Operational Land Imager
S2	Sentinel-2
SCA	Snow Covered Area
SCM	Surface Classification Map
SE	Snow Extent
SLC	Scan Line Corrector
SRTM	Shuttle Radar Topography Mission v4.1
TIRS	Thermal Infrared Sensor
TM	Thematic Mapper
TMSCAG	Thematic mapper snow-covered area and grain size model
TOA	Top of Atmosphere
TOAR	Top of Atmosphere Reflectance
USGS	United States Geological Survey
UTM	Universal Transverse Mercator

VGF	Viewable Gap Fraction
VIS/IR	Visible and infrared
WGS84	World Geodetic System 1984

This page is intentionally left blank.

2. LANDSAT DATASET FOR SNOWPEX

Initially, we selected 459 Landsat scenes from the years 1998 to 2014 for evaluation of medium and low resolution global snow products. After the 2nd ISSPI Workshop, held in September 2015 in Boulder, Colorado, USA, it was decided together with the snow product providers to extend the Landsat reference dataset over the Canadian prairies/Hudson Bay and over Russia. The final reference dataset consists of 498 Landsat scenes which origin from Landsat-5 TM (217), Landsat-7 ETM+ SLC-on (265) and Landsat-8 OLI (16). Figure 2.1 gives an overview of the location and annual availability of the selected scenes. All Landsat data are available in L1T format, meaning that the standard terrain correction using ground control points and a digital elevation model was applied by USGS.

The data are provided to the community via the ENVEO FTP site. A detailed description of the selected Landsat scenes is provided in Deliverable 9.

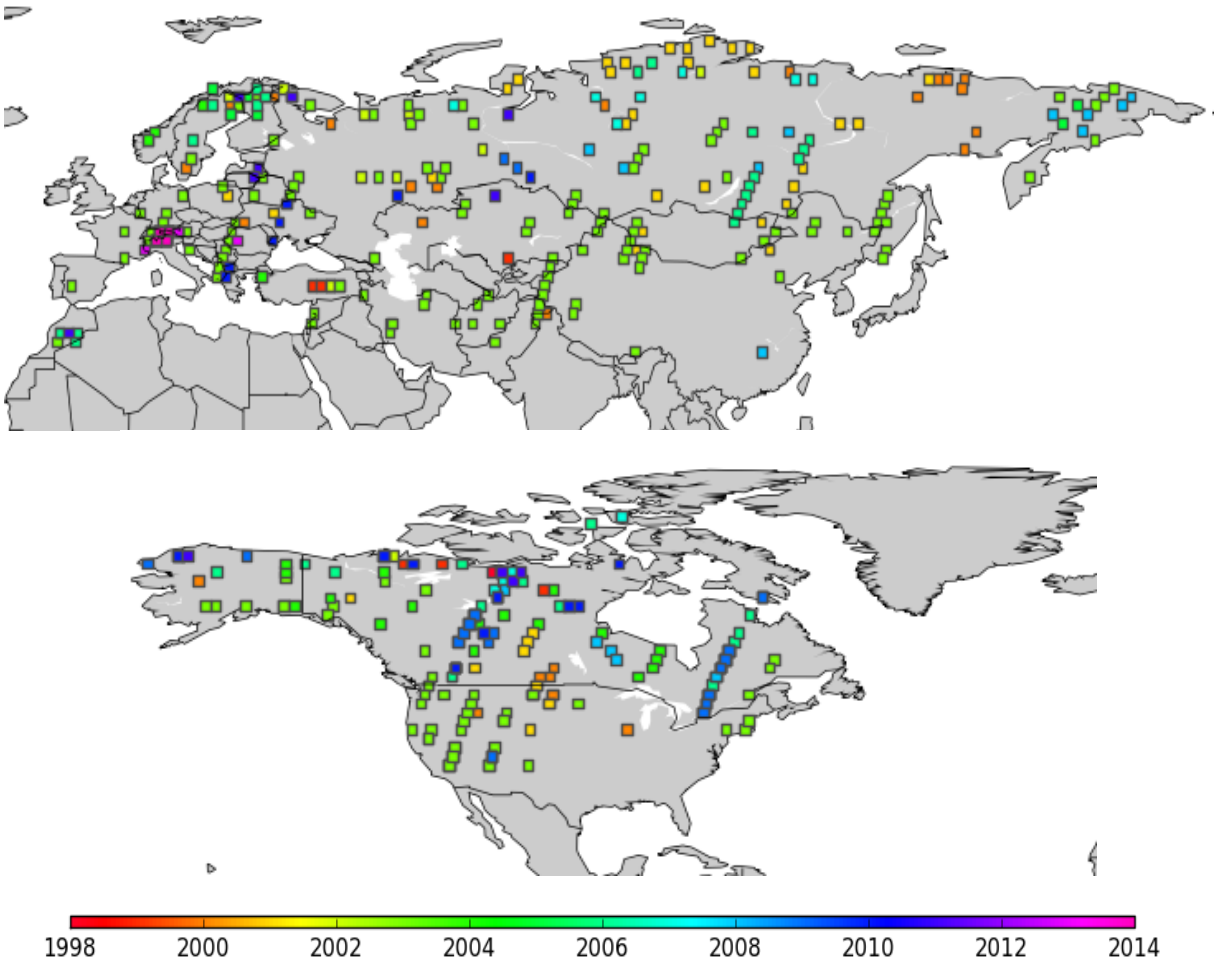

Figure 2.1: Landsat scenes prepared by SnowPEx Consortium with year-dependent colour code (LS data as of 31 March 2016).

This page is intentionally left blank.

3. AUXILIARY DATA

This section provides formation on the used auxiliary data sets required for generation of the Landsat snow reference data set. It includes digital elevation data and maps of surface land cover.

3.1 Digital Elevation Model

A digital elevation model is needed to calculate slope and aspect of the observed terrain required to apply the Ekstrand (1996) topographic correction (see chapter 5.5). The used DEMs for Landsat processing are:

- *EU-DEM* – provides topographic information of European Union countries in 30 x 30 m pixel resolution
- *NED* - National Elevation Dataset over US territory with about 30 x 30 m resolution (1' x 1') or higher, and 2' x 2' resolution for most of Alaska
- *CDED* – Canadian Digital Elevation Data providing elevation information in 0.75" x 0.75" resolution (23 x 16-11 m) and a 15' x 15' cell coverage
- *SRTM v4.*1 – elevation data from 60°N to 60°S and 180°E to 180°W in 90 x 90 m pixel resolution
- *ASTER GDEM2* – topographic information between 83°N and 83°S in 30 x 30 m pixel resolution

The EU-DEM, NED and CDED will be used primary as input data for data processing. Outside the coverage of EU-DEM, NED or CDED, where SRTM v4.1 and ASTER GDEM2 are both available, the SRTM v4.1 is preferred to the ASTER GDEM2, because of known occurrences of pixel artefacts in the ASTER DEM. North of 60°N the ASTER GDEM2 will be used, but has to be manually controlled due to data quality issues. The DEM data type is unsigned integer 16.

3.2 Surface Classification Maps (SCM)

A surface classification mask is needed to discriminate water pixel (open water bodies, rivers and ocean) from land cover to reduce misclassification of water pixels as snow. The input data for producing a land/water mask is:

- *Data Mask* from Hansen et al. (2013), was derived from Landsat scenes and is globally available in 30 x 30 m pixel resolution

- *SRTM Water Bodies* provided as 1°-by-1° tile in ESRI shapefile format (60°N to 60°S and 180°E to 180°W). The data was gathered on SRTM shuttle flights in February 2000. Further specifications can be found in the product documentation files (2003, 2005).

The land/water masks are produced by combining the *Data Mask* with the *SRTM Water Bodies,* resulting in one surface classification map.

Table 3.1:
SCM Coding.

Code range [unsigned byte]	*Class*
0	Land Cover
254	ERROR Code: No satellite data value
255	Not Valid Pixel in Original Projection Products / (e.g. Sea)

3.3 Canopy Closure / Crown Coverage in Landsat 8 OLI / Sentinel-2 MSI resolution

The University of Maryland, Department of Geographical Sciences has produced a global forest change data set based on time-series analysis of Landsat images from 2000 to 2014 (Hansen et.al., 2013). The dataset includes following layers:

- Tree canopy cover for year 2000 (Figure 3.1a), defined as canopy closure for all vegetation taller than 5m in height. Encoded as a percentage per output grid cell, in the range 0–100.
- Global forest cover loss 2000–2014 (loss), defined as a stand-replacement disturbance, or a change from a forest to non-forest state. Encoded as either 1 (loss) or 0 (no loss).
- Global forest cover gain 2000–2012 (gain), defined as the inverse of loss, or a non-forest to forest change entirely within the study period. Encoded as either 1 (gain) or 0 (no gain).
- Year of gross forest cover loss event (lossyear) is a disaggregation of total forest loss to annual time scales. Encoded as either 0 (no loss) or else a value in the range 1–13, representing loss detected primarily in the year 2001–2014, respectively.

Data is available on-line from: http://earthenginepartners.appspot.com/science-2013-global-forest.

The Copernicus High Resolution Layer (HRL) Forest consists of a per-pixel classification of tree cover density and of dominant leaf type. It is based on automated analysis of biophysical parameters derived from multispectral and multi-temporal Earth Observation data from the years 2011 – 2013 (2012 reference year) with 20 m pixel size with interactive editing at the end of the production chain (Büttner, 2012). The Tree Cover Density product (Figure 3.1b) estimates the tree cover as percentage 0-100% with no minimum mapping unit (i.e. pixel resolution of satellite image). The Forest Type product classifies pixels according to the dominant leaf type of tree, in other words to classes 1. broadleaf forest and 2. coniferous forest. The minimum mapping unit is 0.5 ha. The dataset is funded by the European Union, its production controlled by the European Environment Agency and produced by European service providers. Data is available on-line from http://land.copernicus.eu/pan-european/high-resolution-layers/forests/view.

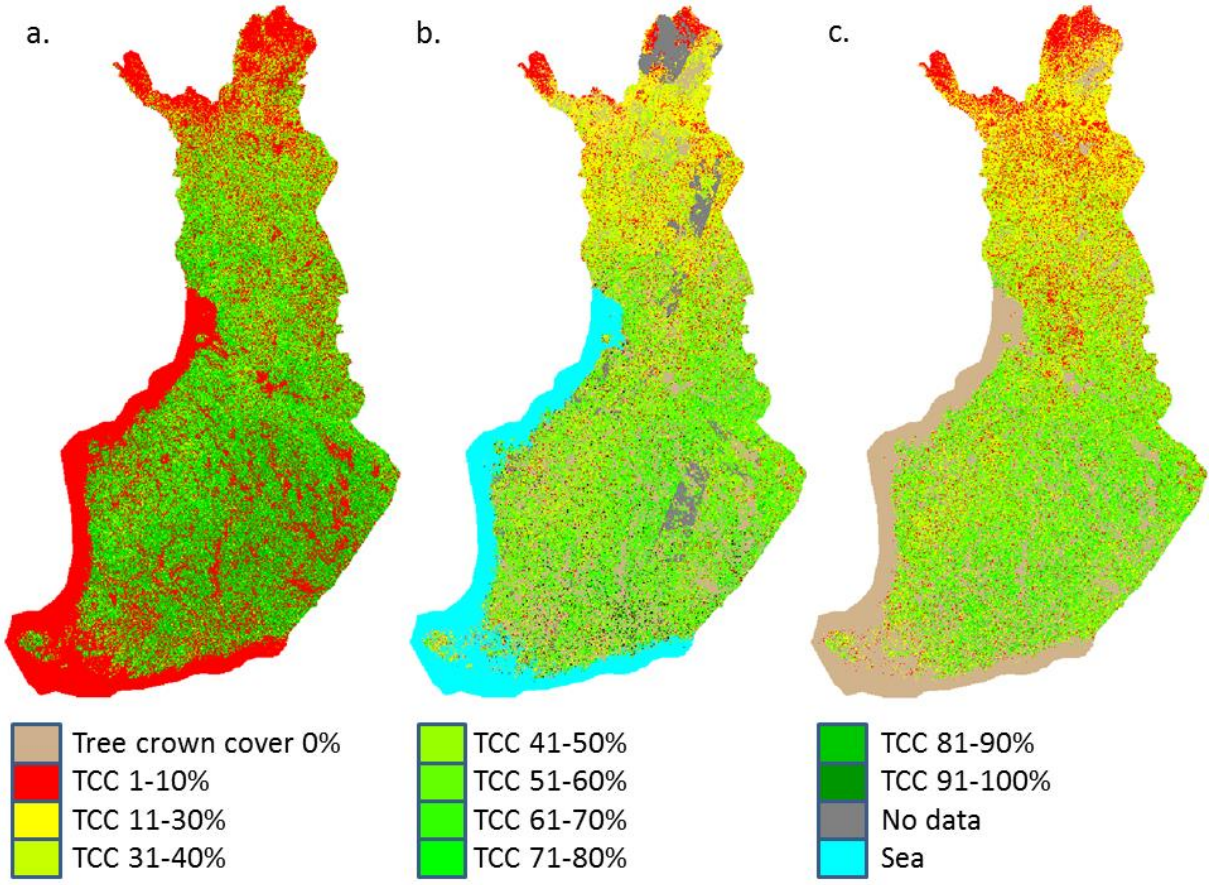

Figure 3.1: Tree crown cover estimates for Finland, a. University of Maryland Tree Canopy Cover 2000, b. Copernicus Land Monitoring HRL Forest Tree Cover Density 2012, and c. Tree crown cover estimate of Finnish National Forest Inventory 2013.

The Finnish National Forest Inventory (NFI) (Tomppo, 2006) by Natural Resources Institute Finland is a monitoring system that produces information concerning national and regional forest resources, health, biodiversity and land use. There are about 70000 sampling plots covering whole Finland (systematic stratified cluster sampling) which are measured every 6 years. In addition to field measurements, the multi-source inventory method employs remote sensing data (Landsat TM/ETM+/OLI, IRS LISS, Spot) and other digital data sources such as land-use maps and elevation models. With the aid of satellite images, the forest characteristics like tree crown cover (Figure 3.1c) and crown cover of deciduous trees can be estimated for areas laying between the relatively sparse network of NFI sample plots. The non-parametric k-nearest neighbour estimation method is used in the image analysis. Map data is used to separate forested areas from other land-cover categories, and peatland maps are used also in stratification. A digital terrain model is used to reduce distortion effects caused by topography. The geometric resolution of both input data and resulting maps is 16 m. The NFI is assumed to be the most accurate tree cover product in Finland due to the high number of in-situ plots used in estimation. Data is available on-line from http://kartta.metla.fi/. In this repot, this dataset is referred to as METLA Crown Coverage (METLA CC).

4. OVERVIEW OF GENERATION OF LANDSAT SNOW REFERENCE DATA SET

Figure 4.1 gives an overview of the Landsat snow maps processing line. All the steps will be described in this document for full transparency and reproducibility of the Landsat reference data set. Each of the snow algorithms is applied on all valid surface classes (from SCM) except water bodies and terrain shadows. Forested areas are not treated separately in the snow map processing, as an algorithm naturally may include a built-in adaptation feature.

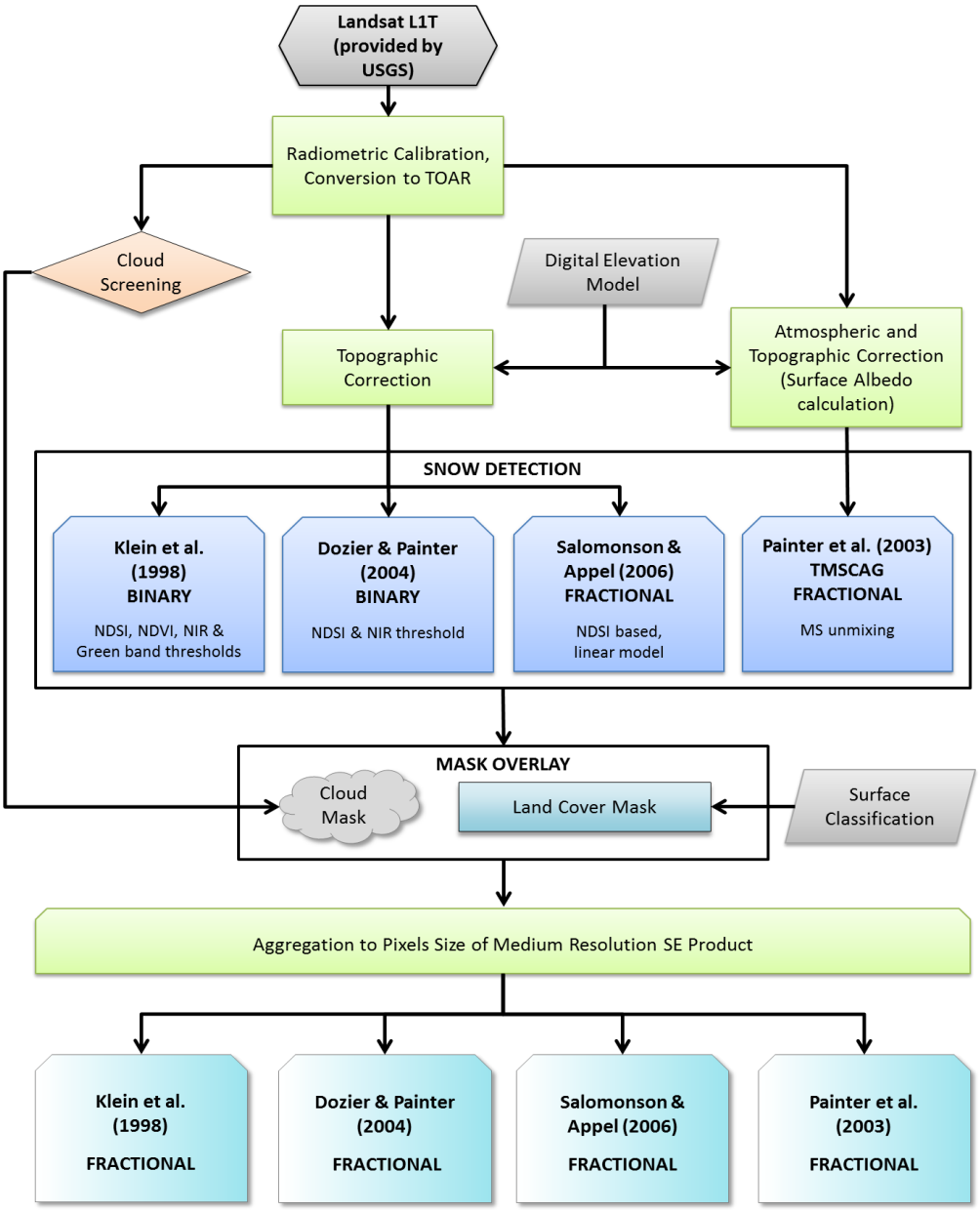

Figure 4.1: Schematic processing line for Landsat snow products within SnowPEx.

All pre-processing steps required for Klein, Dozier and Salomonson algorithms are implemented and processed at ENVEO. The surface reflectance calculation and TMSCAG processing is carried out by T. Painter, K. Rittger and K. Bormann (at NASA JPL, NSIDC).

5. PRE-PROCESSING OF LANDSAT DATA

This chapter describes the specification of Landsat raw data and processing step before snow algorithms are applied.

5.1 Landsat Data Specifications

The Landsat input data originate from different Landsat sensors:

- Landsat-5 Thematic Mapper (TM),
- Landsat-7 Enhanced Thematic Mapper Plus (ETM+) SLC-on and
- Landsat-8 Operational Land Imager (OLI) and Thermal Infrared Sensor (TIRS).

Table 5.1 lists the specifications of the different sensors, such as spectral bandwidth and resolution of the Landsat bands.

Table 5.1:
Band numbers, wavelengths and resolution of Landsat 5, 7 and 8 sensors.

Sensor	*Band No.*	*Spectral Bandwidth (micrometres)*	*Resolution (meters)*
Landsat 5 Thematic Mapper (TM)	Band 1	0.45-0.52	30
	Band 2	0.52-0.60	30
	Band 3	0.63-0.69	30
	Band 4	0.76-0.90	30
	Band 5	1.55-1.75	30
	Band 6	10.40-12.50	120* (30)
	Band 7	2.08-2.35	30
Landsat 7 Enhanced Thematic Mapper Plus (ETM+)	Band 1	0.45-0.52	30
	Band 2	0.52-0.60	30
	Band 3	0.63-0.69	30
	Band 4	0.77-0.90	30

Sensor	*Band No.*	*Spectral Bandwidth (micrometres)*	*Resolution (meters)*
	Band 5	1.55-1.75	30
	Band 6	10.40-12.50	60** (30)
	Band 7	2.09-2.35	30
	Band 8	.52-.90	15
Landsat 8 Operational Land Imager (OLI) and Thermal Infrared Sensor (TIRS) Launched February 11, 2013	Band 1 - Coastal aerosol	0.43 - 0.45	30
	Band 2 - Blue	0.45 - 0.51	30
	Band 3 - Green	0.53 - 0.59	30
	Band 4 - Red	0.64 - 0.67	30
	Band 5 - Near Infrared (NIR)	0.85 - 0.88	30
	Band 6 - SWIR 1	1.57 - 1.65	30
	Band 7 - SWIR 2	2.11 - 2.29	30
	Band 8 - Panchromatic	0.50 - 0.68	15
	Band 9 - Cirrus	1.36 - 1.38	30
	Band 10 - Thermal Infrared (TIRS) 1	10.60 - 11.19	100*** (30)
	Band 11 - Thermal Infrared (TIRS) 2	11.50 - 12.51	100*** (30)

* TM Band 6 was acquired at 120-meter resolution, but products processed before February 25, 2010 are resampled to 60-meter pixels. Products processed after February 25, 2010 are resampled to 30-meter pixels.

** ETM+ Band 6 is acquired at 60-meter resolution. Products processed after February 25, 2010 are resampled to 30-meter pixels

*** TIRS bands are acquired at 100 meter resolution, but are resampled to 30 meter.

5.2 Orthorectification

Landsat images used for snow map processing are level "L1T" products, meaning the scenes are radiometrically and geometrically corrected by USGS, using ground control points and a digital elevation model for the orthorectification. The map projection of the delivered Landsat images is Universal Transverse Mercator (UTM) on WGS84 ellipsoid and will be maintained until pre-processing is finished.

5.3 Pixel Reference and Size

The origin coordinates of all Landsat scenes refer to the upper left corner of the upper left pixel. This pixel reference remains unchanged for all provided snow products. The original Landsat pixel size is 30 m x 30 m and will also be preserved until pre-processing is finished. For algorithms applied by ENVEO, the topographically corrected top of atmosphere reflectance of the Landsat image is then reprojected (bilinear) into the snow extent products coordinate systems (see Table 5.2), from where the snow detection algorithms are applied and the Landsat snow map is aggregated to the snow extent product resolution.

Table 5.2:
Projection of snow extent products participating in SnowPEx (cf. Deliverable D3) and reprojected Landsat pixel size in SE projection.

Projection	Pixel Size in SE Projection	SE Products (SnowPEx PRODID)
Universal Transverse Mercator	30 m x 30 m	EURAC
Geographic Coordinates	0.00025 deg x 0.00025 deg	ASNOW, CRYOL, GLSSE, JXAM5, JXM10
Polar Stereographic Projection	25 m x 25 m	IMS01, IMS04, IMS24
Sinusoidal Projection	25 m x 25 m	M10C05, SCAG
Geostationary Projection	25 m x 25 m	HSAF10, HSAF31
Ease-Grid North	25 m x 25 m	PATHF
Ease-Grid 2.0	25 m x 25 m	CRCLIM, MEASU

5.4 Radiometric Calibration

The Landsat "L1T" data are provided in Digital Numbers (DN) and have to be radiometrically calibrated. Calibration parameters for each band are provided in the associated metadata file (*_MTL.txt) for conversions to at-satellite spectral radiance and top of atmosphere (TOA) reflectance (TOAR) (scaled between 0 and 1) for each band.

For Landsat-5 TM and Landsat-7 ETM+ SLC-on data the at-satellite radiance from calibrated digital numbers (8-bit unsigned integer) is retrieved by the following equation:

$$L_\lambda = \frac{L_{MAX,\lambda} - L_{MIN,\lambda}}{QCAL_{MAX} - QCAL_{MIN}} (QCAL - QCAL_{MIN}) + L_{MIN,\lambda} \qquad \textit{(Equ. 5.1)}$$

Where

- L_λ the spectral radiance at the sensor's aperture in W/(m^2 sr µm)
- $L_{MAX,\lambda}$ is the spectral radiance that is scaled to $QCAL_{MAX}$ in W/(m^2 sr µm)
- $L_{MIN,\lambda}$ is the spectral radiance that is scaled to $QCAL_{MIN}$ in W/(m^2 sr µm)
- $QCAL$ is the quantized calibrated pixel value in DN
- $QCAL_{MAX}$ is the maximum quantized calibrated pixel value (corresp. to $L_{MAX,\lambda}$)
- $QCAL_{MIN}$ is the minimum quantized calibrated pixel value (corresponding to $L_{MIN,\lambda}$)

For the conversion from at-satellite radiance into TOAR, the solar exo-atmospheric spectral irradiance in the specific spectral range of the selected band, the earth – sun distance in astronomical units for the acquisition date, and the solar zenith angle in degrees at the image acquisition are needed. The following equation is used for the conversion:

$$R_t = \frac{L_\lambda \, \pi \, d^2}{E_{sun,\lambda} \cos(\Theta_z)} \qquad \textit{(Equ. 5.2)}$$

Where

- R_t is the top-of-atmosphere reflectance
- L_λ is the spectral radiance at the sensor's aperture in W/(m^2 sr µm)
- d is the sun-earth distance in astronomical units
- $E_{sun,\lambda}$ is the solar constant at a specific wavelength in W/m^2
- Θ_z is the solar zenith angle

For Landsat-8 radiometric calibration is slightly different. The DN are available in 16-bit unsigned integer format and can be directly rescaled optionally to TOA radiance, reflectance or at-satellite brightness temperature with rescaling coefficients provided in the associated metadata file (*_MTL.txt).

For the conversion from DN to TOA radiance the following equation has to be applied:

$$L_\lambda = M_L Q_{cal} + A_L \quad \textit{(Equ. 5.3)}$$

where

- L_λ is the TOA radiance at the sensor's aperture in W/(m^2 sr μm)
- M_L is the band-specific multiplicative rescaling factor from the metadata file (RADIANCE_MULT_BAND_x, x = band number)
- A_L is the band-specific additive rescaling factor from the metadata file (RADIANCE_ADD_BAND_x, x= band number)
- Q_{cal} is the quantized and calibrated standard product pixel values (DN)

For the conversion from DN to TOA reflectance the following equation is used:

$$\rho_\lambda = \frac{M_p Q_{cal} + A_p}{\cos(\Theta_z)} = \frac{M_p Q_{cal} + A_p}{\sin(\Theta_s)} \quad \textit{(Equ. 5.4)}$$

where

- ρ_λ is the TOA reflectance
- M_p is the band-specific multiplicative rescaling factor from the metadata file (REFLECTANCE_MULT_BAND_x, x = band number)
- A_p is the band-specific additive rescaling factor from the metadata file (REFLECTANCE_ADD_BAND_x, x= band number)
- Q_{cal} is the quantized and calibrated standard product pixel values (DN)
- Θ_z is the local solar zenith angle; $\Theta_z = 90° - \Theta_s$
- Θ_s is the local sun elevation angle provided in the metadata file (SUN_ELEVATION))

5.5 Topographic Correction

The processing line of Landsat snow products includes "Ekstrand" correction (Ekstrand, 1996) which is applied to the TOA reflectance to correct for topographically induced effects and atmospheric propagation. "Ekstrand" topographic correction was found to be most suitable over complex mountainous terrain (Bippus, 2011) and is described by following equation:

$$L_h = L_t * \left(\frac{\cos(\Theta_s)}{\cos(i)}\right)^{k*\cos(i)} \quad \textit{(Equ. 5.5)}$$

where

- L_t is the reflectance on an inclined surface
- L_h is the quivalent reflectance on a horizontal surface
- Θ_s is the solar zenith angle
- i is the solar illumination angle in relation to a normal on a pixel
- k is the Minnaert constant (0.0 < k < 1.0)

By applying *Equ. 5.6,* we assume that the atmospheric path radiance is low compared to radiance from the surface.

In 2 cases Ekstrand's approach is not valid:

- if cos(i) < 0 (self shadow) and
- if a pixel is shadowed by an adjacent pixel.

Thresholds applied to detect dark and shadowed surfaces support the determination of selection of valid pixels for snow classification (Section 0). Optionally, a terrain shadow mask could be generated based on the DEM and solar elevation provided in the metadata file of the satellite data as auxiliary mask for snow map processing.

5.6 Cloud Detection

This section describes the cloud screening for Landsat images. Initially the Landsat scenes are manually classified into 5 cloud classes described in Table 5.3. The cloud screening is done automatically applying the ACCA.SEAS algorithm developed by Chris Crawford (NASA), which is an improved version of the Automatic Cloud Cover Assessment (ACCA). The retrieved cloud masks are visually checked, and manually corrected if needed. In case the cloud screening is not applicable for a Landsat scene the cloud masking will be performed manually.

ACCA.SEAS

The ACCA.SEAS algorithm is an unsupervised classifier detecting clouds taking advantage of the spectral properties of clouds, snow, bright soil, vegetation, and water. A VIS/IR spectral signature for

cold clouds is developed during the processing to evolve a thermal profile for cold and warm clouds. Further brightness temperatures are used to screen ambiguous warm clouds including an added seasonal discrimination to account for thermal variability. Cloud shadows are detected taking the solar geometry at the acquisition date and time into account. The resulting cloud/shadow mask is finally filtered to flag out cloud edges and holes.

Three binary cloud maps are produced by the ACCA.SEAS cloud screening approach: a cloud mask, a cloud shadow mask and a combined cloud/cloud shadow mask.

The cloud screening algorithm performs best over mid-latitude regions and during the spring season. Therefore, it will be tested and mainly applied on Landsat scenes with these regional and temporal specifications.

Table 5.3:
Cloud classification for Landsat scenes and applied cloud detection methods.

Cloud Classes		***Scenes***
0	completely clear-sky; no need for cloud masking	205
1	clouds concentrated in a certain part of scene area; masking by hand easy (and necessary)	137
2	very few scattered clouds; masking a bit laborious; however, if not done, does not affect the result very much	39
3	scattered clouds and shadows; masking laborious but has to be done if using the scene	78
4	too cloudy for intercomparison / cloud masking very laborious	-

Cloud Map Coding

Code range [unsigned byte]	***Class***
0	Cloud free
205	Clouds and cloud shadow

This page is intentionally left blank.

6. SNOW MAP GENERATION FROM LANDSAT DATA

This chapter describes the snow detection algorithms for Landsat snow map processing used as reference data for snow extent product evaluation. The snow algorithms used are listed in Table 6.1. Snow algorithms are only applied on valid land pixels excluding water bodies derived from the Surface Classification Mask (Section 3.2).

Table 6.1:
Landsat binary and fractional snow detection algorithm.

Algorithm	*Reference*	*BIN/FSC*	*Thematic information*	*Required AUX data*	*Section*
Dozier	Dozier and Painter (2004)	BIN	Snow on ground	DEM,SCM	6.3.1
Klein	Klein et al. (1998)	BIN	Snow on ground	DEM,SCM	6.3.2
Salomonson	Salomonson and Appel (2004,2006)	FSC	Viewable snow	DEM,SCM	6.3.3
TMSCAG	Painter et al. (2003)	FSC	Viewable snow, snow on ground	DEM	6.3.4

6.1 Snow Map Coding

The coding of the Landsat snow maps corresponds to the snow map coding of the medium resolution snow products selected for the intercomparison activities in the SnowPEx project.

Table 6.2:
Coding of snow maps from Landsat data.

Code range	*Class*
0-100	Fractional: snow cover fraction in per cent Binary: 0 = snow free; 100 = fully snow covered
205	Clouds (incl. cloud shadow) Note: snow retrieval not possible due masking of earth surface
206	Polar Night / satellite data available, but polar night does not allow classification

Code range	*Class*
207	Cast shadows and dark surface pixel
252	ERROR Code: Retrieval / Classification failed
253	ERROR Code: Input data error (e.g. bad pixels, etc)
254	ERROR Code: No satellite data value
255	Not Valid Pixel in Original Projection Products / (e.g. Sea)

6.2 Common Pre-Processing Steps

Additional to the approaches described in Section 6.3 two conditions were accomplished beforehand on Landsat scenes (except for TMSCAG).

Thermal threshold (optional)

A threshold is applied on the thermal band of Landsat in order to reduce misclassifications due to bright warm surface classes, as for instance bright warm rocks (Metsämäki et al., 2015):

if $BT_{11\,\mu m} > 288\ K$ *then* ***NO SNOW***

Shadow and dark surface threshold

For detecting cast shadowed areas and dark surfaces (e.g. undetected water bodies) additional thresholds are applied on the visible band at 0.55 µm, the mid infrared band at 1.6 µm, and on the Normalized Difference Vegetation Index (NDVI):

$$NDVI = \frac{REF_{0.85\mu m} - REF_{0.66\mu m}}{REF_{0.85\mu m} + REF_{0.66\mu m}} \qquad \textit{(Equ. 6.1)}$$

Non-valid pixels are classified if the following conditions are met:

if $REF_{1.6\,\mu m} < 0.02$ *and* $REF_{0.55\,\mu m} < 0.2$ *and* $NDVI < 0.1$

then ***NO VALID PIXEL***

6.3 Landsat Snow Mapping Algorithms

6.3.1 Binary SE by adapted method after Dozier and Painter (2004)

The approach of Dozier and Painter (2004) for snow classification is based on thresholds applied on the Normalized Difference Snow Index (NDSI, Hall et al., 1995) and on the near-infrared band at 0.85 µm:

$$NDSI = \frac{VIS-SWIR}{VIS+SWIR} = \frac{REF_{0.55\ \mu m} - REF_{1.6\ \mu m}}{REF_{0.55\ \mu m} + \mathrm{REF}_{1.6\ \mu m}} \qquad \textit{(Equ. 6.2)}$$

The following condition is used for classifying binary snow:

if ***NDSI > 0.40*** *and* ***$REF_{0.85\ \mu m}$ > 0.11*** *then* ***SNOW***

The resulting snow map provides binary information on snow on ground.

Based on experiences of former validation activities, by applying this method on Landsat scenes in different climate zones, changing solar illumination and surface conditions the NDSI threshold eventually has to be modified to resolve better high resolution snow reference data. Modifications and adaptions of the applied algorithm will therefore be documented in a separate logfile.

6.3.2 Binary SE by adapted method after Klein et al. (1998)

The method of Klein et al. (1998) is based on applying thresholds to the NDSI (Equ. 6.2) and the NDVI (Equ. 6.1) and spectral queries (Poon, 2004 and Poon and Valeo, 2006).

if ***$REF_{0.55\mu m}$ > 0.10*** *and* ***$REF_{0.85\mu m}$ > 0.11***

AND some of the following is true:

→ ***NDSI > 0.4*** *or*

→ ***NDVI ≥ 0.25*** *and* ***NDSI ≥ 0.0652 * EXP(1.8069 * NDVI)*** *or*

→ ***NDVI ≥ 0.1*** *and* ***NDVI < 0.25*** *and* ***NDSI ≥ (NDVI-0.2883)/-0.4828)***

THEN ***SNOW***

OTHERWISE pixel is ***SNOW FREE***

The resulting snow map provides binary information on snow on ground.

6.3.3 Fractional SE by adapted method after Salomonson and Appel (2006)

The method of Salomonson and Appel (2006) is based on the Normalized Difference Snow Index (NDSI, Equ. 6.2). The approach uses a linear model to weight the binary snow classification derived by the NDSI:

$$FSC = -0.01 + 1.45 * NDSI \quad \textit{(Equ. 6.3)}$$

For calibrating the weighting values a set of Landsat and MODIS data sets over various surface types and with varying snow conditions was analysed and set into relation.

The resulting snow map provides fractional information on viewable snow.

6.3.4 Fractional SE and grain size Algorithm (SCAG) after Painter et al. (2003)

Landsat ETM+ and TM frequently saturate over snow in bands 1 through 3, resulting in a spectrum with artificially low apparent reflectance in the visible wavelengths. The Landsat fractional snow cover is estimated using a spectral mixing model similar to MODSCAG (Painter et al., 2009, Rittger et al., 2013), but accounting for various combinations of saturation in the ETM+ visible bands (bands 1, 2, and 3). In these Landsat snow cover maps, four saturation scenarios can occur over snow: (i) none, in conditions of low illumination or shadows; (ii) just band 1 (0.45–0.515 μm), (iii) bands 1 and 3 (0.630–0.690 μm), and (iv) bands 1, 2 (0.525–0.605 μm), and 3. Therefore, when the three visible bands are saturated, 100% snow cover is assumed. This assumption can represent an overestimate if subpixel rock or vegetation is present, but this is the most reasonable assumption with the given information. In the scenarios of bands 1 and 3 saturated or band 1 only saturated, a spectral mixture analysis is performed on the remaining bands.

The code was developed with surface reflectance estimated from the 6S model (Kotchenova et al., 2006; Kotchenova & Vermote, 2007), tailored to incorporate a digital elevation model to vary the atmospheric optical thickness. Currently it is run using USGS climate data record (CDR) surface reflectance. Evaluations using 0.4m WorldView-2 imagery (Rittger, et al, SnowPEx ISSPI-2 workshop, 2015) show similar snow mapping performance using the two different surface reflectance estimates in five test cases in Colorado, California (2), Utah, and Iceland considering both binary and fractional error estimates.

A detailed description of the algorithm is given e.g. in Painter et al (2003).

The snow map resulting from the standard method provides fractional information on viewable snow.

Additionally, a provisional Landsat product that was adjusted in forest has been created to address evaluation of coarse resolution “snow on the ground” products using the equation:

$$f_{SCA}^{(adjusted)} = \frac{f_{SCA}^{(viewable)}}{VGF} \approx \frac{f_{SCA}^{(viewable)}}{1-f_{VEG}} \qquad \textit{(Equ. 6.4)}$$

where VGF is the viewable gap fraction. This product provides fractional information on snow on ground, but has not been evaluated yet.

Due to the complexity of TMSCAG, the algorithm was not implemented within SnowPEx. Snow products based on TMSCAG (visible snow and canopy corrected snow on ground) were by courtesy made available by the algorithm developers Thomas Painter and his group, especially Karl Rittger and Kat Bormann.

These snow products are provided in UTM / WGS84 map projection, and are then reprojected and aggregated to the map projection and pixel size of the global/hemispheric products to be validated.

This page is intentionally left blank.

7. RESAMPLING METHOD OF HIGH RESOLUTION SNOW MAPS

Landsat binary and fractional snow maps are resampled to the grid size of the snow product they are going to be validated with. Therefore, the method applied for resampling is averaging the snow pixel to the desired resolution:

$$FSC_{lr} = \frac{\sum_{hr=1}^{N} FSC_{hr}}{N} \qquad \textit{(Equ. 7.1)}$$

where FSC_{lr} is the resampled averaged fractional snow cover (values between 0 and 100 %), FSC_{hr} is the fractional snow cover of the high resolution image pixels falling within a given low resolution (LR) grid cell (values between 0 and 100 %), and *N* is the number of high resolution (HR) pixels needed for covering the LR grid cell.

There are two cases where not all HR pixels that are part of a LR grid cell are valid FSC pixel:

- invalid HR pixels and
- unmapped HR pixels.

Invalid HR pixels are pixels outside of the mapping domain of FSC products in general, like oceans or water bodies. Those pixels derived from the Surface Class Map are excluded from the snow map generation from HR satellite data.

Unmapped HR pixels correspond to all other conditions where a FSC estimate is not provided. Those pixels are for example cloud pixel (Cloud Mask), cast shadow pixel (Terrain Shadow Mask) or pixel where no satellite data is available.

If invalid and unmapped pixels are present in sufficient quantities in a LR pixel, the LR pixel will be eliminated from evaluation. Therefore, a separate “Resample Map” (in LR) is generated to estimate percentage (%) of invalid and unmapped pixels separately.

This page is intentionally left blank.

8. LANDSAT OUTPUT LAYERS

8.1 High Resolution Maps

For each available snow extent product and its coordinate system, the reference snow products from Landsat data are generated with the four algorithms described in Chapter 0:

- Dozier and Painter (2004) (implemented and processed by ENVEO)
- Klein et al. (1998), (implemented and processed by ENVEO)
- Salomonson and Appel (2004, 2006) (implemented and processed by ENVEO)
- TMSCAG - Painter et al. (2003) (products provided by T. Painter, K. Rittger & K. Bormann)

In the retrieved snow maps cloud cover and water bodies are masked.

8.2 Medium/Low Resolution Maps

The snow maps from Landsat data are aggregated to the medium resolution (ranging from 0.5 km to 5 km) of the global / hemispheric snow extent products. The resampling method is described in Chapter 7.

This page is intentionally left blank.

9. QUALITY ASSESSMENT OF LANDSAT SNOW MAPS

9.1 Method

In order to exploit the 4 snow algorithms applied on Landsat scenes for evaluation of coarse resolution snow extent products it has been decided at the ISSPI-2 Workshop to check how the snow maps generated by these LS algorithms differ from each other after aggregation to 1 km and 5 km according to following methodology:

- Aggregate Landsat snow maps (25 m pixel size in Geographic Coordinates) to 1 km and 5 km pixel sizes
- Calculate the average of FSC, use spreading as uncertainty measure

For each of the Landsat scenes information on the forest content from GlobCover in geographic coordinates on WGS84 ellipsoid will be provided by the SnowPEx team.

The different **thematic information** (viewable snow, snow on ground, cf. Table 6.1) provided by the 4 algorithms applied on the Landsat scenes has to be considered for the evaluation of the global/hemispheric snow extent products **in forested areas**. **All 4 Landsat algorithms are applied on all non-forested areas**.

9.2 Intercomparison of Landsat Snow Algorithms

The LS algorithm intercomparison is performed using only clear sky images due to the availability of the SCAG LS FSC snow maps only for those scenes. The intercomparison is performed for the total Landsat image (without taking surface classes into account) (Figure 9.1) and also split up into comparisons of unforested (Figure 9.2) and forested (Figure 9.3) areas due to the different quantities (viewable snow or snow-on-ground) the Landsat snow algorithms are detecting in forested areas.

The pixel-by-pixel intercomparisons of the Landsat image area is performed by aggregating the original Landsat snow maps to 1 and 5 km to achieve FSC maps for all LS snow maps and compare them at lower resolutions. The results between 1 and 5 km haven't shown much difference from each other therefore only the results of the intercomparison at 5 km are described.

Figure 9.1 shows the bias and unbiased RMSE of intercomparison between all algorithms over the total image area. The grey shaded areas in the figure show the results of intercomparison of Landsat algorithms detecting different quantities. The snow-on-ground detecting algorithms (Klein, Dozier and

TMSCAGca) have a high agreement between each other with a low bias especially between Klein and TMSCAGca of -0.18 and a low RMSE of 6.6. The viewable snow algorithms from Salomonson and TMSCAG demonstrate that the TMSCAG detects in general less snow cover than Salomonson with a bias of -6.4 which might result from different approaches in the snow detection algorithm (Salomonson is based on NDSI and TMSCAG is based multispectral snow detection). Although Salomonson and Dozier claim to detect different quantities the intercomparison shows a high agreement between both algorithms.

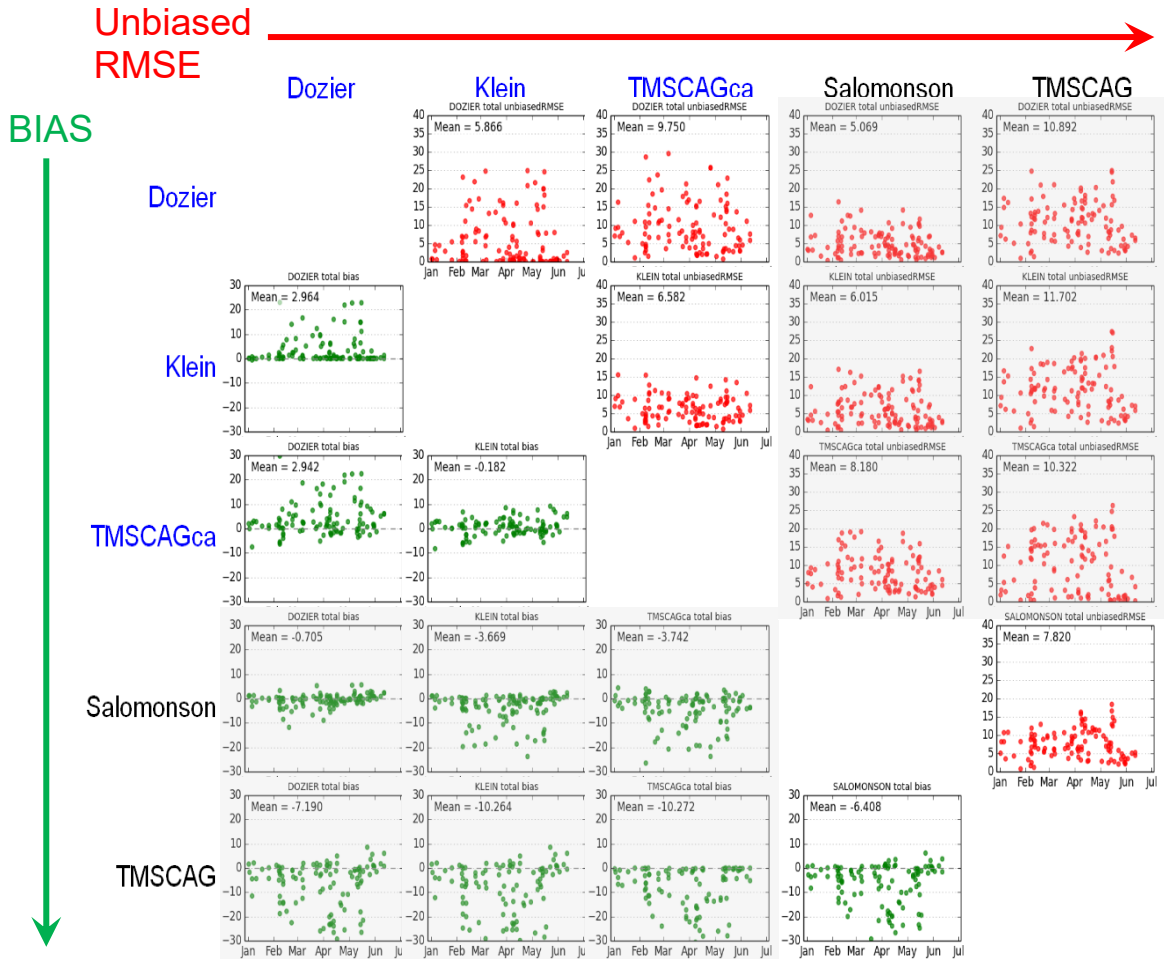

Figure 9.1: Landsat snow algorithms intercomparison over the total Landsat snow map area for the period January to July including **all surface classes**. Blue font: Algorithms detecting snow-on-ground, black font: algorithms detecting viewable snow. Grey shaded are intercomparisons of Landsat scenes measuring different quantities.

Looking into the effect of different surface classes, we focused on unforested/open areas (Figure 9.2) where all algorithms are directly comparable. All algorithms beside TMSCAG show a high agreement between each other with biases between -2 and 2. TMSCAG has the overall tendency to detect less snow over open areas compared to the other algorithms (bias between -4 and -6).

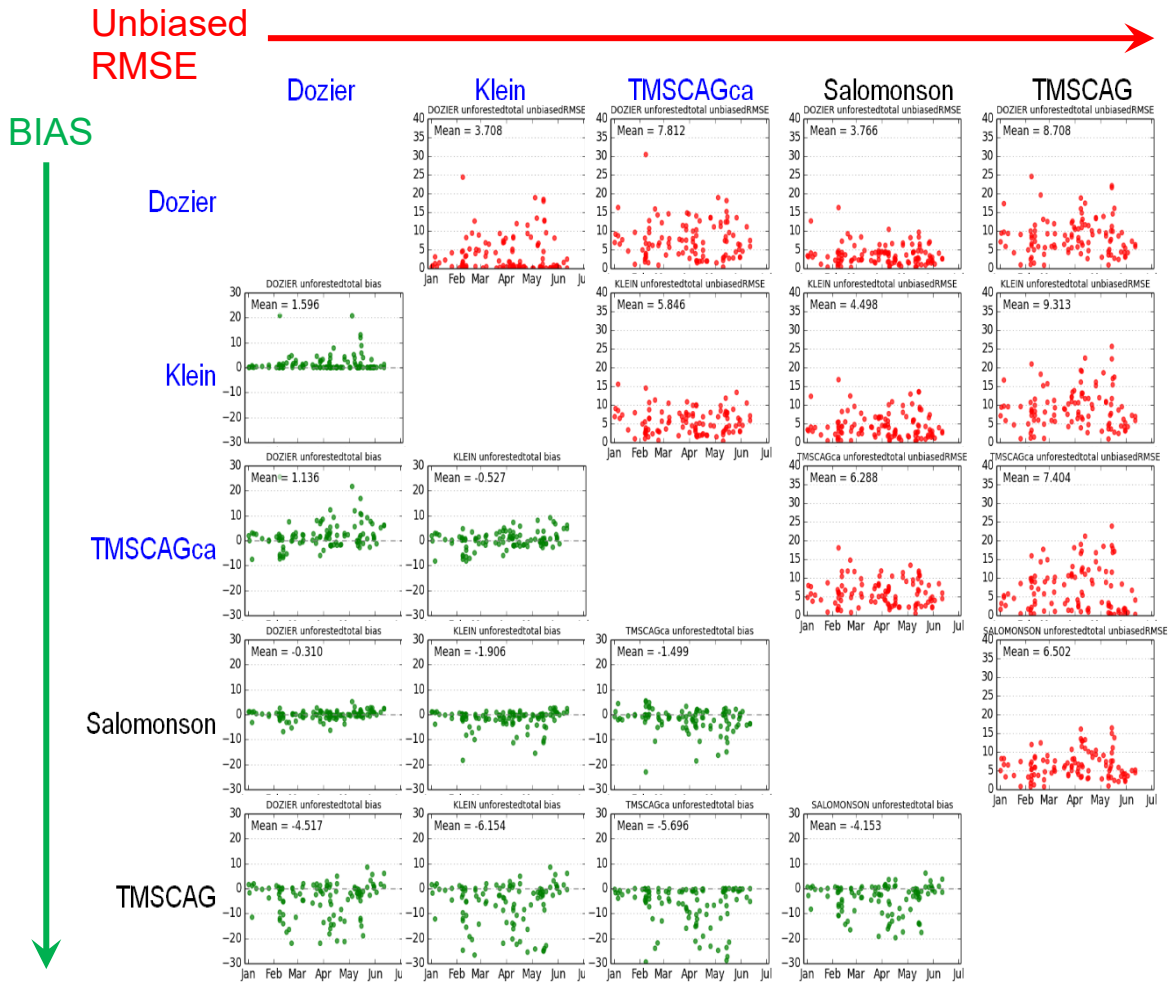

Figure 9.2: Landsat snow algorithms intercomparison over the total Landsat snow map area for the period January to July over **unforested** areas. Blue font: Algorithms detecting snow on ground, black font: algorithms detecting viewable snow.

Whereas the algorithms show a high agreement in unforested areas, detecting snow in forests or snow on top of the canopy is critical (Figure 9.3). Different approaches in the LS snow algorithms result in quite different amount of snow for forested areas. Comparisons of Klein vs. Dozier or TMSCAca vs. Dozier show less snow cover in the Dozier algorithm. TMSCAGca and Klein detect almost the same amount of snow throughout the whole intercomparison period. Regarding the viewable snow detection algorithms Salomonson detects in general more snow with bias of 9.3 although compared

to the other algorithms the unbiased RMSE is low ranging between 0 and 15. All the results of the total or forested/unforested surface classes show no seasonal trend in detecting less or more snow as shown here for the winter or spring season.

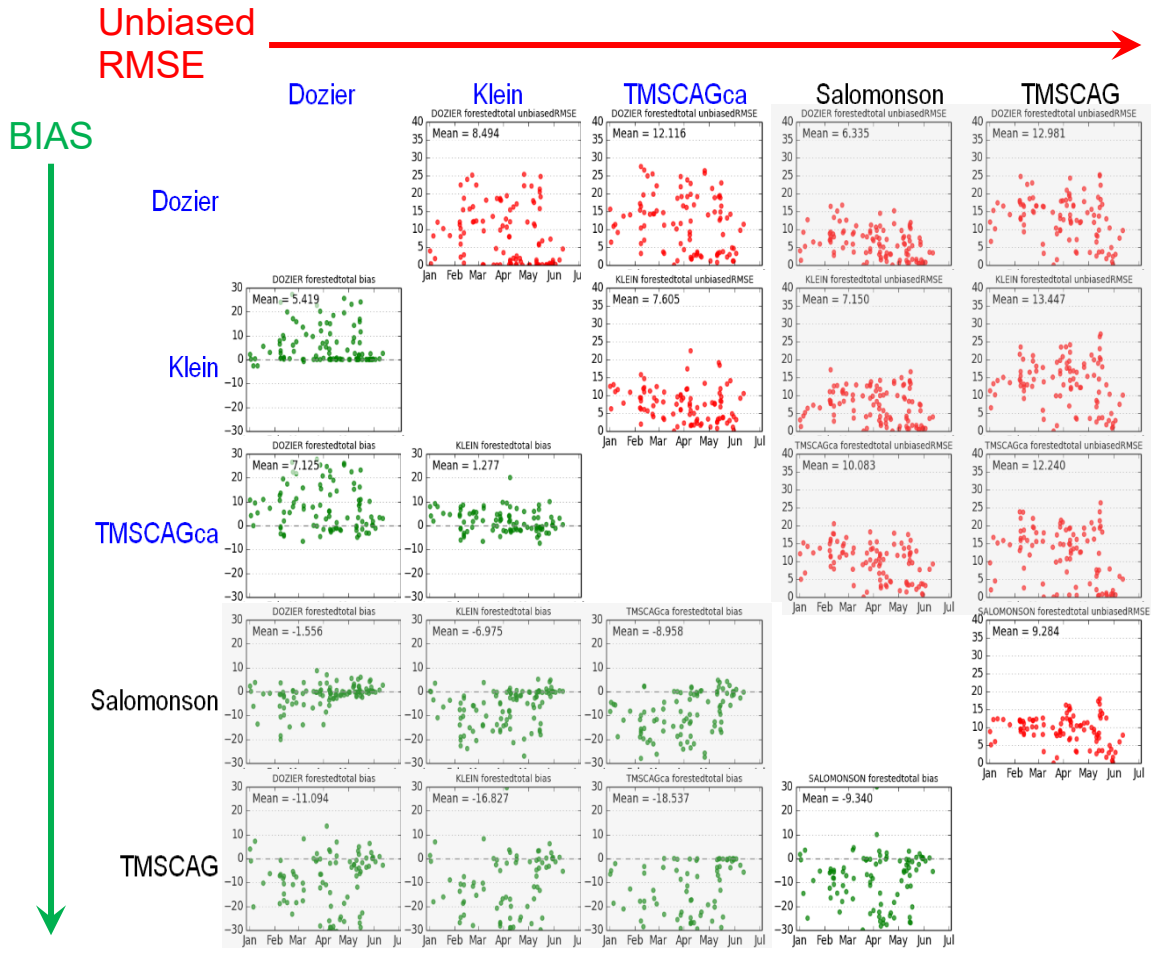

Figure 9.3: Landsat snow algorithms intercomparison over the total Landsat snow map area for the period January to July over **forested** areas. Blue font: Algorithms detecting snow on ground, black font: algorithms detecting viewable snow. Grey shaded are intercomparisons of Landsat scenes measuring different quantities.

10. DEVELOPMENT OF NEW METHODS FOR HIGH RESOLUTION SNOW MAPS FROM LANDSAT OR SENTINEL-2

The Sentinel-2 (S2) satellite, launched on 23 June 2015, offers new possibilities in snow cover detection in an even higher resolution than the Landsat satellite series. The spectral bands are similar to the Landsat satellites but Sentinel-2's MSI provides even more spectral bands and information in the visible spectrum at 10 and 20 m resolution (Figure 10.1).

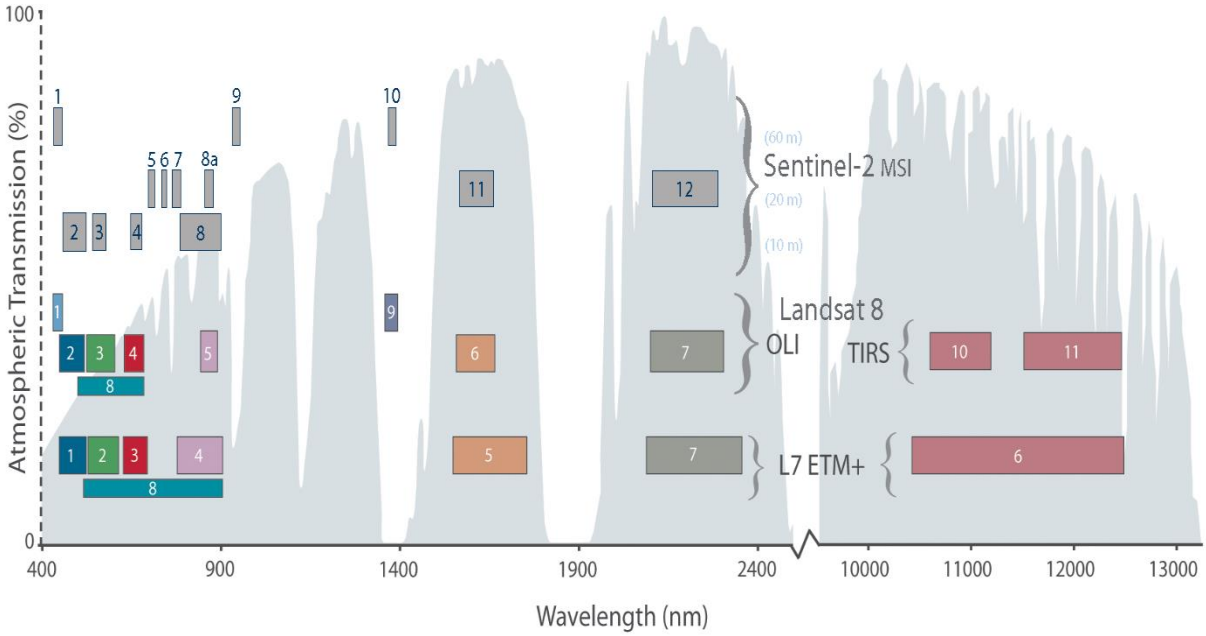

Figure 10.1: Spectral range of Landsat-7 and Landsat-8 bands in comparison to Sentinel-2 bands (USGS).

S2 acquires all the necessary bands for the implemented snow detection algorithms (Figure 10.2) except for the thermal band at 11 µm which is used to support the discrimination of snow and bright rocks (see chapter 0). Hence, we excluded the usage of the thermal band option from the initial tests.

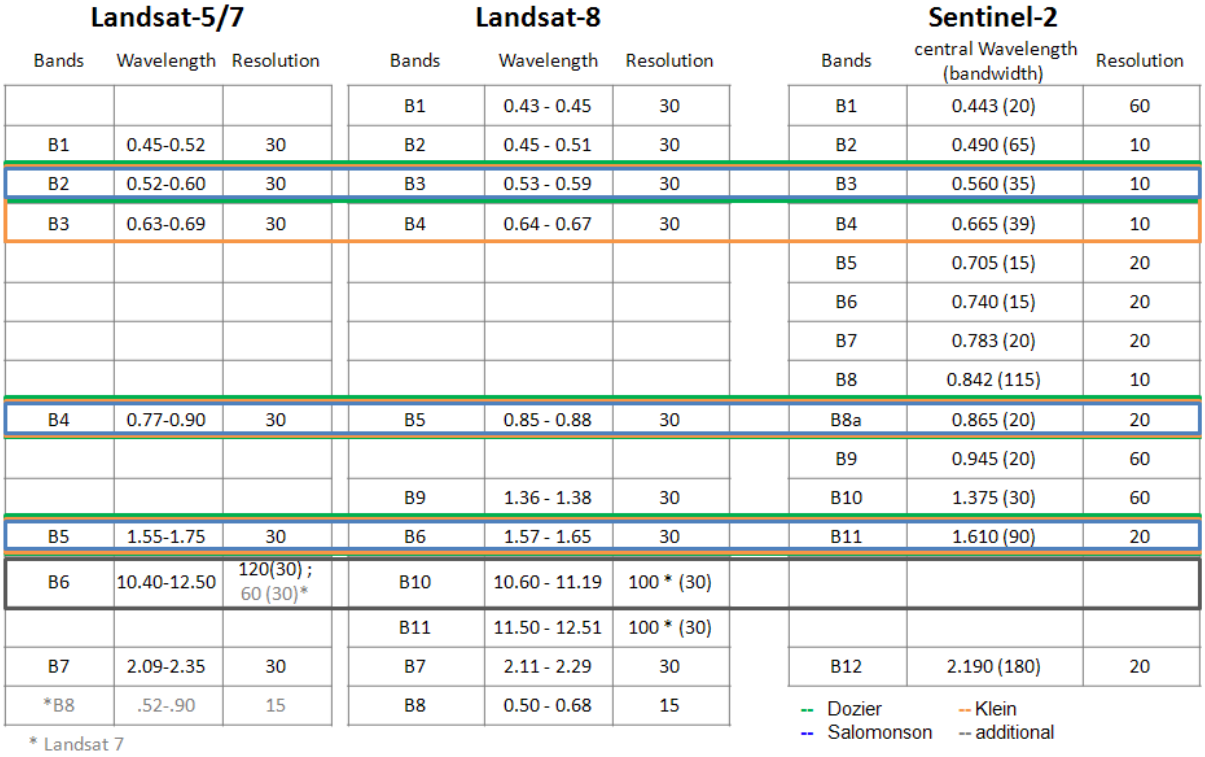

Landsat-5/7			Landsat-8			Sentinel-2		
Bands	Wavelength	Resolution	Bands	Wavelength	Resolution	Bands	central Wavelength (bandwidth)	Resolution
			B1	0.43 - 0.45	30	B1	0.443 (20)	60
B1	0.45-0.52	30	B2	0.45 - 0.51	30	B2	0.490 (65)	10
B2	0.52-0.60	30	B3	0.53 - 0.59	30	B3	0.560 (35)	10
B3	0.63-0.69	30	B4	0.64 - 0.67	30	B4	0.665 (39)	10
						B5	0.705 (15)	20
						B6	0.740 (15)	20
						B7	0.783 (20)	20
						B8	0.842 (115)	10
B4	0.77-0.90	30	B5	0.85 - 0.88	30	B8a	0.865 (20)	20
						B9	0.945 (20)	60
			B9	1.36 - 1.38	30	B10	1.375 (30)	60
B5	1.55-1.75	30	B6	1.57 - 1.65	30	B11	1.610 (90)	20
B6	10.40-12.50	120(30) ; 60 (30)*	B10	10.60 - 11.19	100 * (30)			
			B11	11.50 - 12.51	100 * (30)			
B7	2.09-2.35	30	B7	2.11 - 2.29	30	B12	2.190 (180)	20
*B8	.52-.90	15	B8	0.50 - 0.68	15			

Figure 10.2: Intercomparison of bands from Landsat-5/7/8 and Sentinel-2 regarding using implemented Landsat snow map detection algorithms from Dozier, Salomonson and Klein for Sentinel-2.

10.1 Test data

For testing purposes of the new snow map algorithms, Sentinel-2 and Landsat 8 scenes over the Austrian Alps of the winter season 2015/2016 and Landsat 8 data over Finland acquired in 2013, 2014 and 2015 were selected. Any cloud covered areas on the selected scenes were masked manually.

Table 10.1:
Landsat and Sentinel-2 data sets selected for testing new methods for snow detections from high resolution satellite data.

REGION	*ENTITY ID*	*ACQUISITION DATE (YYYY-MM-DD)*	*SENSOR*	*CENTRE LAT*	*CENTRE LON*	*CLOUDS*
Alps	LC81920272015365LGN00	2015-12-31	OLI	47.44921 N	12.59576 E	24 %

REGION	ENTITY ID	ACQUISITION DATE (YYYY-MM-DD)	SENSOR	CENTRE LAT	CENTRE LON	CLOUDS
Alps	S2A_OPER_PRD_MSIL1C_PDMC_ 20151231T180112_R022_ V20151231T102248_20151231T102248	2015-12-31	MSI	47.31009 N	12.37201 E	39 %
Alps	S2A_OPER_PRD_MSIL1C_PDMC_ 20160216T135146_R022_ V20160130T101456_20160130T101456	2016-01-30	MSI	47.34138 N	11.05061 E	34 %
Finland	LC81910132014099LGN00	2014-04-09	OLI	66.93918 N	26.15371 E	1 %
Finland	LC81910132015070LGN00	2015-03-11	OLI	66.93898 N	26.19723 E	0 %
Finland	LC81900132013137LGN01	2013-05-17	OLI	66.93916 N	27.77243 E	1 %

10.2 Snow map generation in mountainous terrain

10.2.1 Preparatory work

In a first step to develop a new algorithm for mountainous regions the S2 snow detection capability was tested with the already implemented algorithms from Salomonson, Klein and Dozier. Therefore, all S2 bands were oversampled to 10 m pixel resolution, converted to TOA reflectance and Ekstrand topographic correction was applied. Figure 10.3 shows the test site 'Hohe Tauern' in the Austrian Alps as a false colour composites of S2 and LS-8.

The S2 and LS-8 scenes were acquired on the same date, with about 25 minutes difference in the image acquisition time. Figure 10.6 and Figure 10.7 show the results of S2 snow maps in comparison to LS-8 snow maps generated with the Klein and the Salomonson algorithms, respectively.

Zooming to a smaller subset of the S2 and LS-8 scenes demonstrates the difference in the resolution in the snow detection of both sensors (Figure 10.6, Figure 10.7).

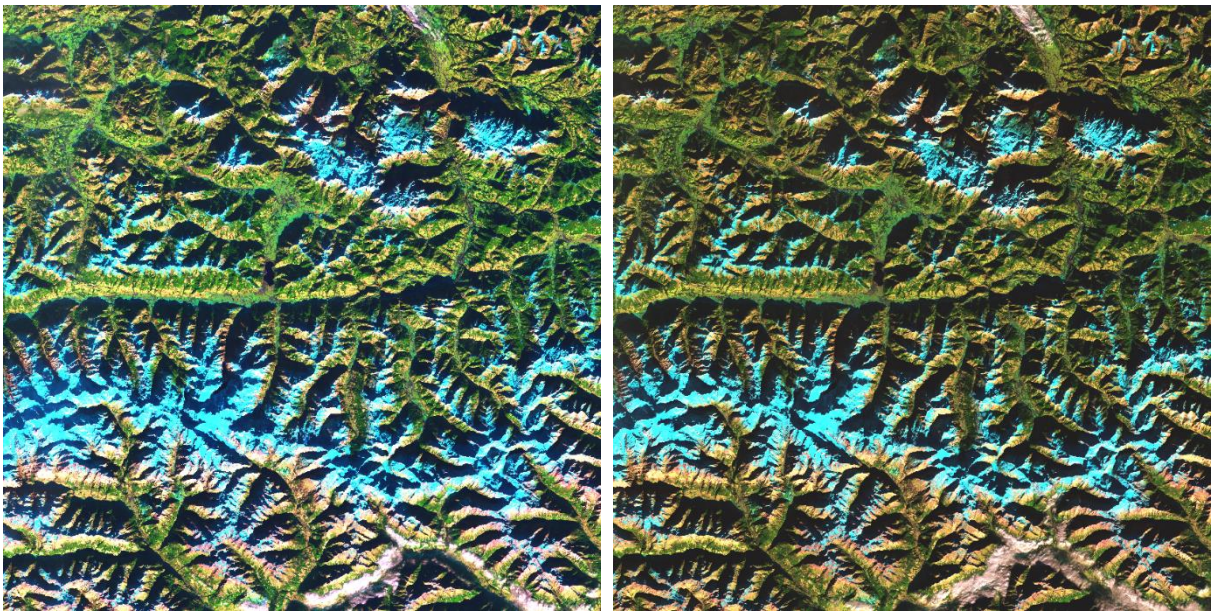

Figure 10.3: Sentinel-2 and Landsat 8 false colour composites over the region Hohe Tauern, Austria, of 31 December 2015. Left: Sentinel-2 (R022, T32TQT) RGB 11-8A-4, 10 m, scene start time: 10:22:48.936Z. Right: Landsat-8 (192/027) RGB 6-5-4, 30 m, scene centre time: 09:58:04.7208940Z.

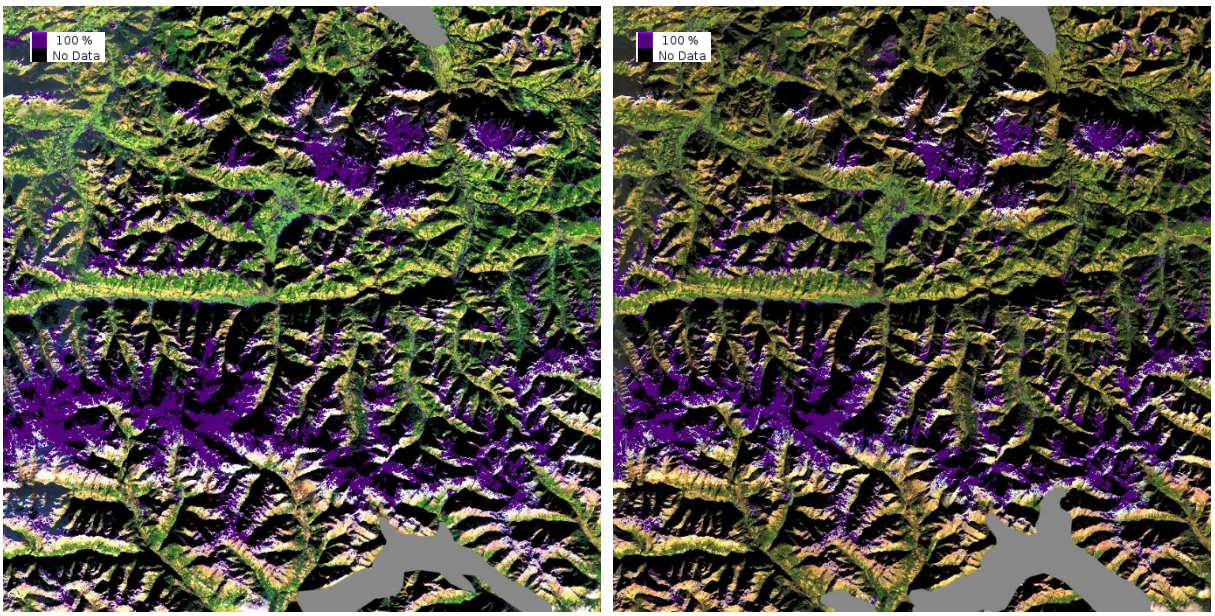

Figure 10.4: Binary snow maps calculated with Klein algorithm from Sentinel-2 and Landsat-8 of 31 December 2015. Left: S2 snow map in 10m resolution, right: LS-8 snow map in 30 m resolution. Grey areas show cloud masks.

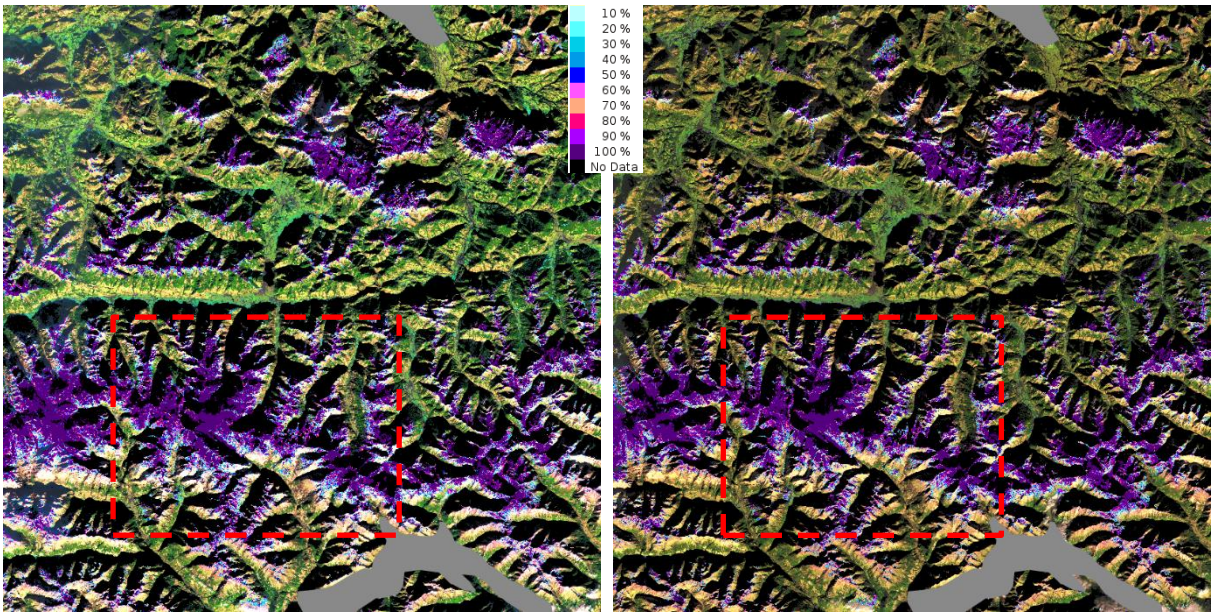

Figure 10.5: Fractional snow maps calculated with Salomonson algorithm from Sentinel-2 and Landsat-8 of 31 December 2015. Left: S2 snow map in 10m resolution, right: LS-8 snow map in 30 m resolution. The red dashed outlines indicate the location of the subsets shown in Figure 10.6 and Figure 10.7. Grey areas show cloud masks.

Visual intercomparisons of S2 and LS-8 snow maps from Salomonson algorithm shows a more detailed snow cover fraction for the higher resolved image from S2 (Figure 10.7). As expected, all 3 implemented snow detection algorithms can be used as already implemented for snow mapping from S2 without additional adaption for the spectral bands (no misclassification in snow detection due to different bandwidths, etc.).

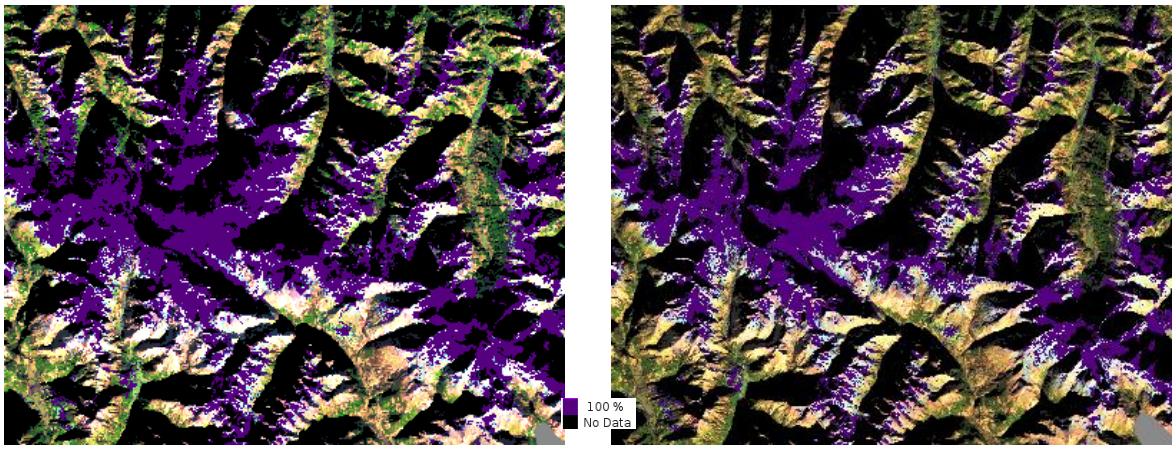

Figure 10.6: Subsets of the binary snow maps calculated with Klein algorithms from S2 (left, 10 m) and LS-8 (right, 30 m) scenes of 31 December 2015. Grey areas show cloud masks.

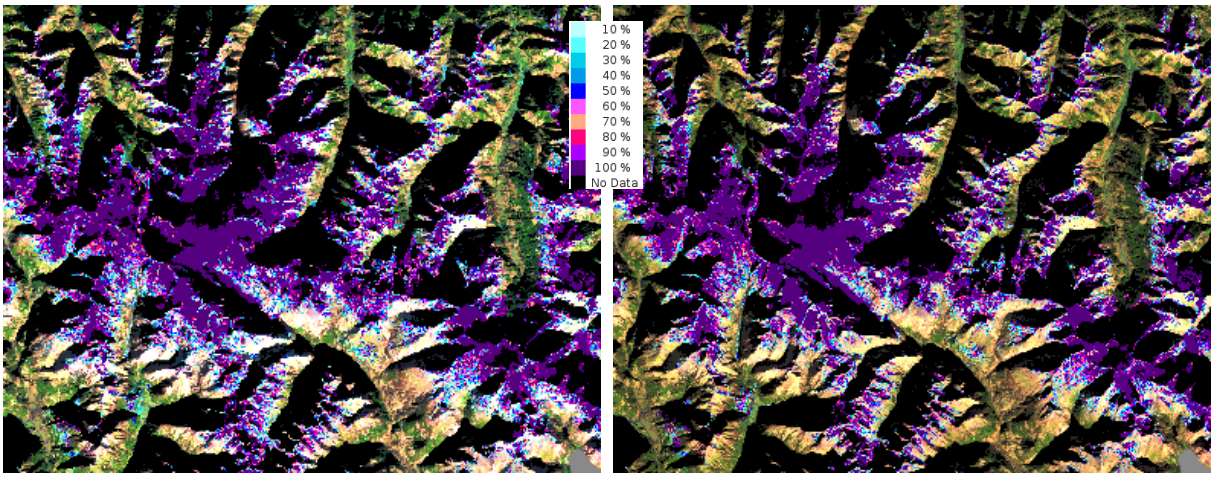

Figure 10.7: Subsets of the fractional snow maps calculated with Salomonson algorithms from S2 (left, 10 m) and LS-8 (right, 30 m) scenes of 31 December 2015. Grey areas show cloud masks.

As a second step we applied a multispectral un-mixing algorithm developed for mountainous terrain using all spectral applicable bands from S2 (excluding cirrus and water vapour bands). The algorithm is based on multispectral un-mixing with end-member selection and was initially developed at ENVEO (Nagler et al., 2012) within the project ASaG, funded by the 6th call of the Austrian Space Applications Programme of FFG / BMVIT, for detecting fractional snow cover in unforested high-alpine areas.

10.2.2 Fractional SE using multispectral un-mixing with end-member selection

The multispectral un-mixing algorithm exploits the different spectral signatures of snow in the visible and infrared spectral ranges. For unforested areas 2 end-members are detected: fully snow covered and completely snow free pixels. This binary classification is performed using the NDSI (Equ. 6.2) and applying a threshold to the TOA reflectance at 0.66 µm.

The fully snow covered and completely snow free pixels are identified according to the following rules:

if (NDSI ≥ 0.7 and R_{TOA}(0.66µm) > 11.0 %) then 100 % SNOW
else if (NDSI < 0.1 and R_{TOA}(0.66µm) ≤ 5.0 %) then SNOWFREE
else MIXED PIXEL (MULTI-SPECTRAL UN-MIXING APPLIED)

The fractional snow cover of the "mixed pixel" is classified applying multi-spectral linear un-mixing with local end-member selection. The nearest 5 snow covered and 5 snow free pixel are used as end-members and are selected in by a helical search (Figure 10.8).

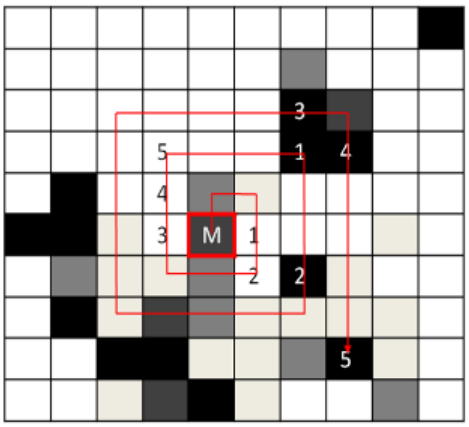

Figure 10.8: End-member selection for mixed pixels. “M” indicates the observed mixed pixel.

For each combination of snow covered and snow free pixels (25) the linear spectral un-mixing is performed and the combination showing the smallest difference between calculated and measured reflectance (ε_λ) is defined as output:

$$R_\lambda = \sum_{i=1}^{M} F_i . R_{\lambda,i} + \varepsilon_\lambda \qquad \textit{(Equ. 10.1)}$$

- R_λ = Reflectance of the pixel of wavelength λ
- $R_{\lambda,i}$ = Reflectance of end-member i and wavelength λ
- F_i = Fraction of end-member i
- ε_λ = Residual error at wavelength λ

In forested areas the different reflectance behaviour causes difficulties mainly resulting in an underestimation of FSC. Therefore, only a binary snow classification (snow in forest and snow-free forest) is performed using NDSI thresholding as described. The forest mask from Hansen et al. (2013) is used as input to discriminate between open land and forest cover. Because the multispectral un-mixing algorithm is developed for unforested high-alpine areas, we decided to apply the Salomonson algorithm to the pixels classified as 'snow in forest' resulting in a FSC detection also in the forested areas (Figure 10.9).

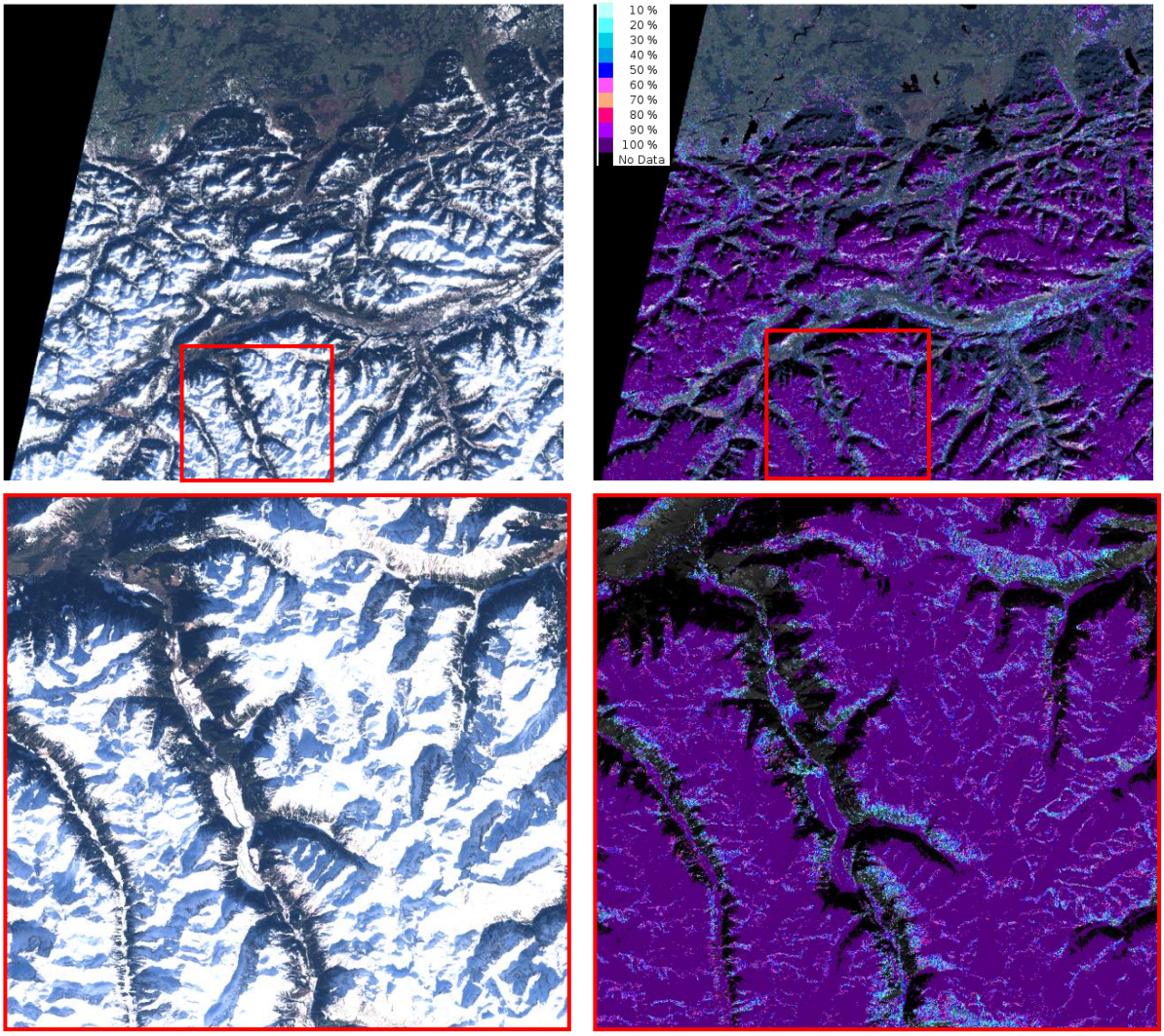

Figure 10.9: Left: Sentinel-2 (T32TPT) colour composite RGB 11-8A-4. Right: FSC map from Sentinel-2 applying multispectral un-mixing (open areas) and Salomonson algorithm (forest covered areas) in 10 m pixel resolution on 30 January 2016.

10.3 Snow map generation in boreal forested areas

10.3.1 Fractional SE using SCAmod

SCAmod is a zeroth-order radiative transfer-based reflectance model to calculated fractions of snow covered area (SCF) in each image pixel. The method relies on pre-determined information of forest canopy transmissivity (range 0-1) and pre-determined values for three major reflectance constituents: forest canopy, melting (wet) snow and snow-free ground (Metsämäki et al., 2005; 2012). The

applicability of SCAmod is not really scale dependent, so the development of SCAmod for high-resolution data such as Landsat-8 OLI and S2/MSI may well rely in it. The basic assumption is that given the transmissivity in the corresponding resolutions and using the suitable values for the three reflectance contributors SCAmod is using, we are able to provide SCF also in the high resolution (in this case about 25 m).

10.3.2 Preparation of transmissivity in the resolution of LS-8 OLI/S2 MSI

Generation of transmissivity for a pixel basically relies on the use of SCAmod so the transmissivity is solved from using at-satellite (TOA) reflectance observations acquired under full snow conditions beneath canopy. This allows the exclusion of unknown variables of SCF (since 100 % snow cover is observed) and calculation of transmissivity reduces into a liner equation (Metsämäki et al., 2005):

$$t_\lambda^2 = \frac{\rho_{\lambda,obs}\,(FSC=1) - \rho_{\lambda,forest}}{\rho_{\lambda,\mathrm{snow}} - \rho_{\lambda,forest}} \qquad \textit{(Equ. 10.2)}$$

- $\rho_{\lambda,snow}$= reflectance of melting snow
- $\rho_{\lambda,forest}$ = dense forest canopy reflectance
- $\rho_{\lambda,ground}$ = reflectance of snow-free ground

It is obvious that for extensive areas, preparing a LS-8/S2 scene specific transmissivity from reflectance observations would be a very laborious task. Therefore, we developed a method which relates information of canopy closure (or Crown Coverage) to the transmissivity in certain study areas. These parameters are denoted as CC in this chapter. Since S2/MSI were not available by the time of conducting the study, we used LS-8/OLI data for the analyses. First, OLI reflectance observations under full snow cover conditions were employed to calculate a transmissivity map for test scenes located in the Finnish Lapland in the area surrounding to Sodankylä Arctic Research Centre FMI/Arc. LS-8 scenes (path 191, row 013) were employed from different acquisition dates, one from 09 April 2014 and another from 11 March 2015. Neither of these scenes represents the situation of at fresh dry snow, so an applicable snow reflectance was extracted from the figures by investigating their histograms and by detecting the confident snow free areas. As a result, we found that snow reflectance of 0.754 (75%) was generally suitable for transmissivity calculations, given the basic idea that only one generally applicable value was to be used instead of spatially varying one. Reflectances for forest canopy and snow-free ground follow the values specified earlier for e.g. GlobSnow or CryoLand, as they should not be scale dependent and we applied the same wavelength band as with those one, i.e. 550 nm (band 2 of LS-8/OLI). Accordingly, $R_{snow\text{-}free}$ = 0.010 and R_{canopy} = 0.08 (see e.g. Metsämäki et al., 2015) were considered to be feasible. Three transmissivity maps were obtained for the study area: *1)* for 09 April

2014, *2)* for 11 March 2015, and *3)* their average. Since the differences of the former two were very small, it was decided to continue studies with the averaged map, shown in Figure 10.10.

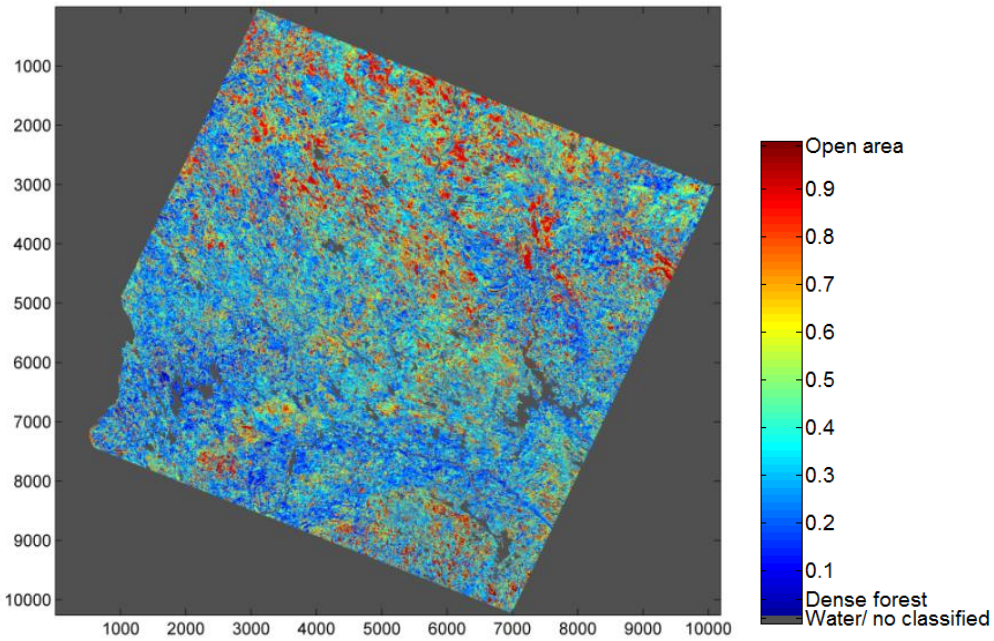

Figure 10.10: Average transmissivity (t^2) for the LS-8 scene 191/013 of 9 April 2014 and 11 March 2015, Finnish Lapland.

10.3.3 Building a model between CC and transmissivity

Canopy Closure is available from different sources. We used three different data sources: 1) CC from the national forest inventory by METLA, available only for Finland 2) Copernicus high resolution layer (HRL) forest, available for Europe and 3) University of Maryland crown coverage data (Hansen et al. 2013), see Sections 3.2 and 3.3 for details.

The analysis was first made from METLA CC data, as it is considered to be the most accurate of these ones. The accuracy was further verified by comparing all three CC data against the CC information gained from high resolution (10m) LIDAR-based CC map for a test area in Finnish Lapland, and METLA CC shows inevitably best agreement with that. The pre-calculated LS-8 data based transmissivity was compared against Canopy Closure data from i) Metla VMI and ii) Copernicus HRL. The analyses were made separately for deciduous dominant pixels (CC of deciduous forest > 75% of the total CC of a pixel) and conifer-dominant pixels (CC conifer forest > 75 % of the total CC of the pixel) and finally, for all land pixels independent of the forest type.

The final goal is to derive a model between the CC data and the transmissivity; for this purpose, CC data were divided into intervals to avoid the influence of large difference between number of cases at

different CC-levels. By averaging the transmissivities within intervals, building a model is clearly easier and more independent on the number of cases: as a results we got the mean and standard deviation (std) for transmissivity for each interval. The final model was fit to these mean values.

The analyses between METLA CC and transmissivity is presented in Figure 10.11. The number of cases in each CC-interval is shown (Top Left), as well as the scatterplot accompanied by blue exponential fit line for all the data points and the error bars (mean ± std) for transmissivity for the CC-intervals (Top Right). The bottom image shows the same data set but now as a density image which clearly better visualized the relationship between CC and transmissivity. The same error bars are presented, but here the exponential fit line (white) is calculated from the average transmissivities for CC-intervals. This is the final fit line to be employed to convert CC to transmissivity for another LS-8 scene.

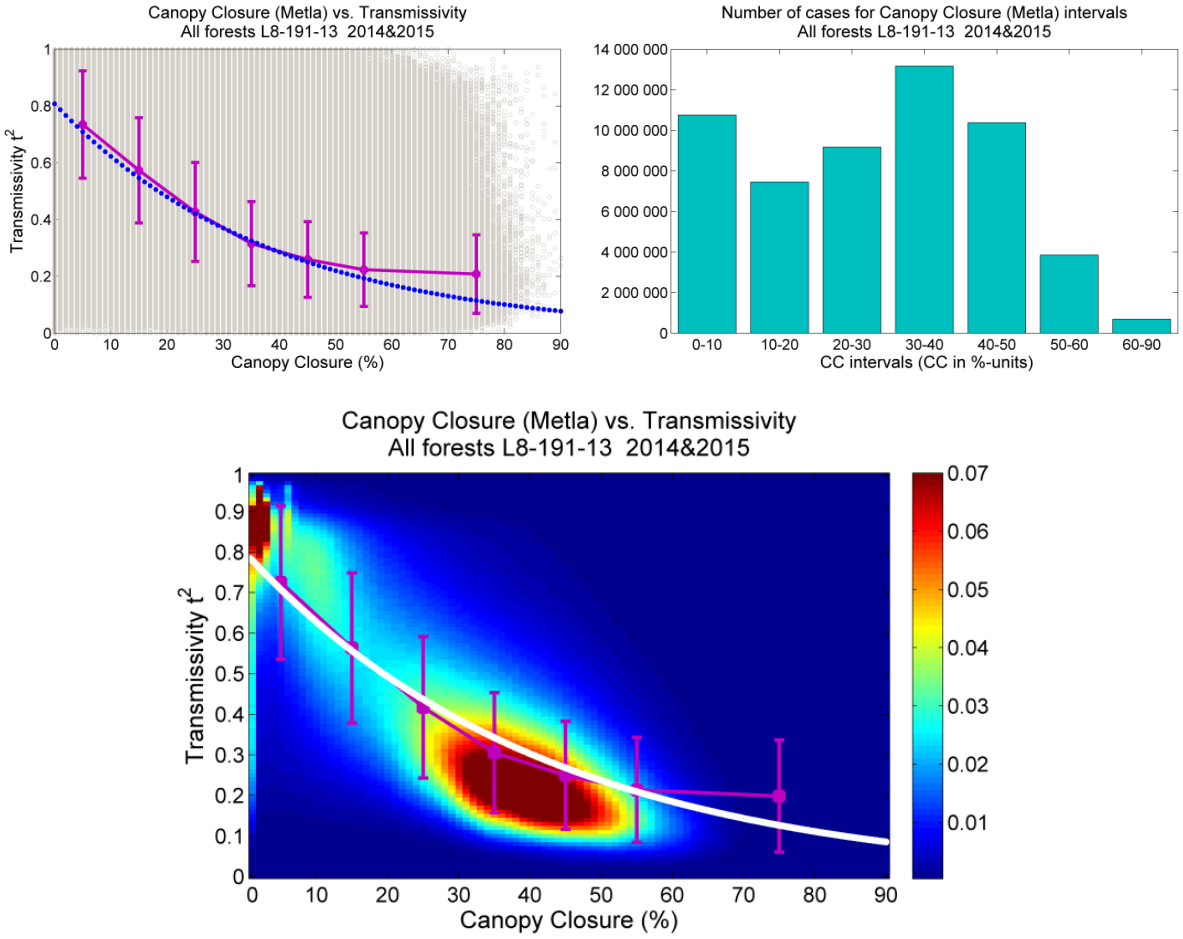

Figure 10.11: For all land pixels with Canopy Closure (CC) ranging from 0 to 100%. *Top Left:* Number of pixels within CC categories; *Top Right:* scatterplot CC vs. transmissivity with exponential model fit to the data (blue line, with also mean and standard deviation of transmissivities falling within each CC interval, *Bottom:* Density plot of the data and the exponential model fit to the average transmissivities for CC intervals. The colour bar indicates the percentage of cases when CC/transmissivity-space is divided in 100×100 grid.

Figure 10.12 depicts the gained models generated between Canopy Closure and the transmissivity, separately for conifer and deciduous forest and in general. The model obtained for Copernicus HRL deciduous differs clearly from the other models, and the models are more or less diverged in general. Therefore, particularly since the deciduous/conifer discrimination may be problematic in the CC datasets, we decided to use a common model for all forests, regardless if they are conifer or deciduous dominant. This decision is supported by the fact that the combined models both for Copernicus HRL CC and METLA CC are very close to each other.

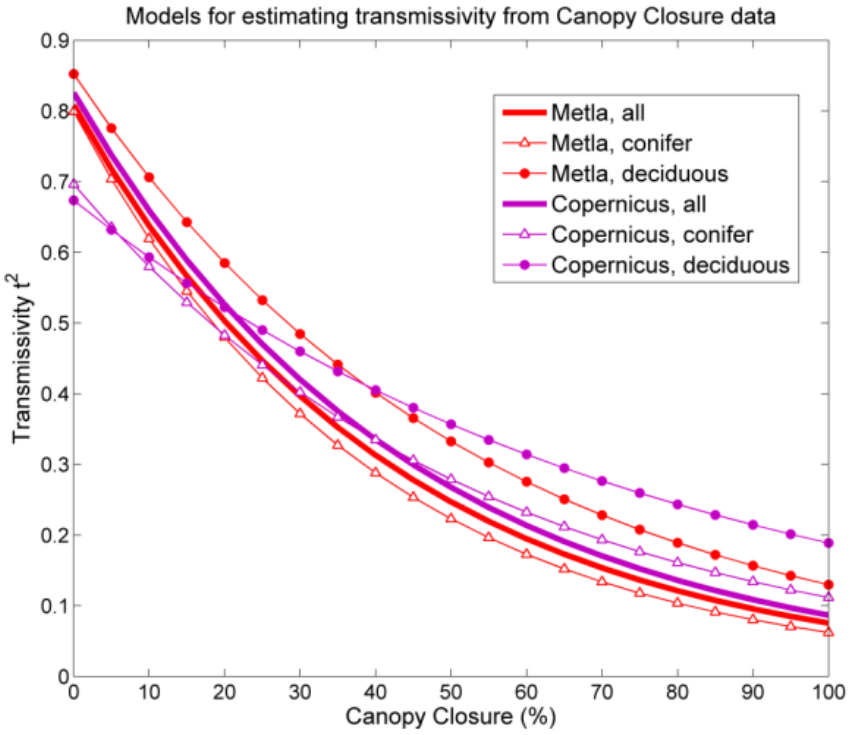

Figure 10.12: Models build between LS-8-dervied transmissivity and Canopy Closure data.

Two models, one from METLA CC and another from Copernicus HRL CC were employed to produce a transmissivity map for the LS-8 scene 191/013 i.e. the very same one as used in creating the model. The results are presented in Figure 10.13. There are slight differences between these two transmissivity maps, but in general they agree quite nicely. The defect in the Copernicus HRL CC data is that is has some large gaps in the areas.

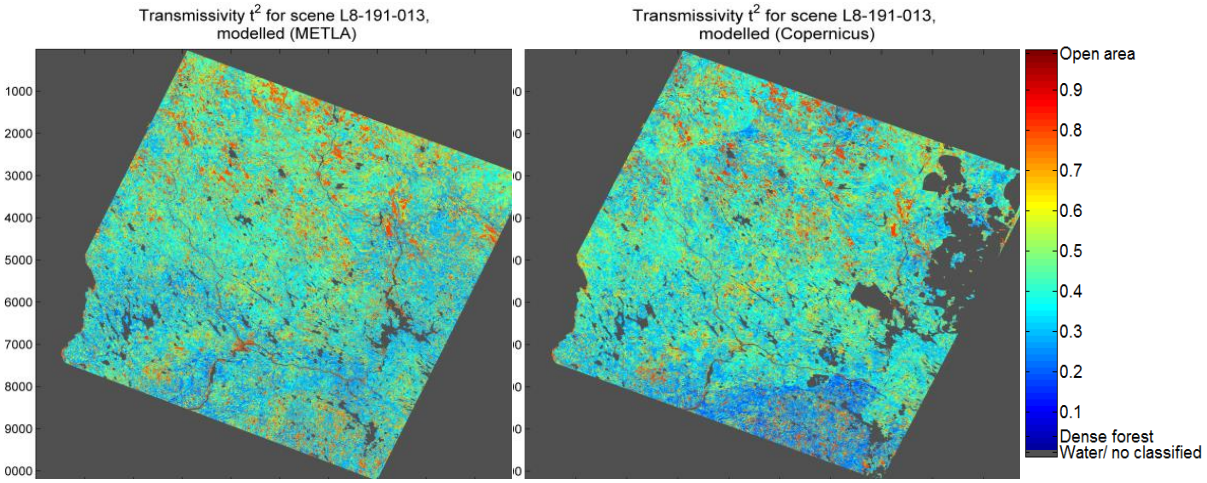

Figure 10.13: Transmissivity map for scene area LS-8/191/013 using modelled Canopy Closure (crown coverage) → transmissivity conversion; *Left:* Metla CC applied, *Right:* Copernicus HRL CC applied. The large dark grey areas in the right-hand-side map are due to the gaps in Copernicus HRL CC data.

10.3.4 Transmissivity maps generated using the gained model

The first test for transmissivity generation outside the above described training scene was made for a LS-8 scene (190/13) of 17 May 2013. Transmissivities were generated using CC METLA and CC Copernicus HRL; after this, SCAmod was applied to produce Fractional Snow Cover (FSC) maps. The resulting FSC-maps are presented in Figure 10.14.

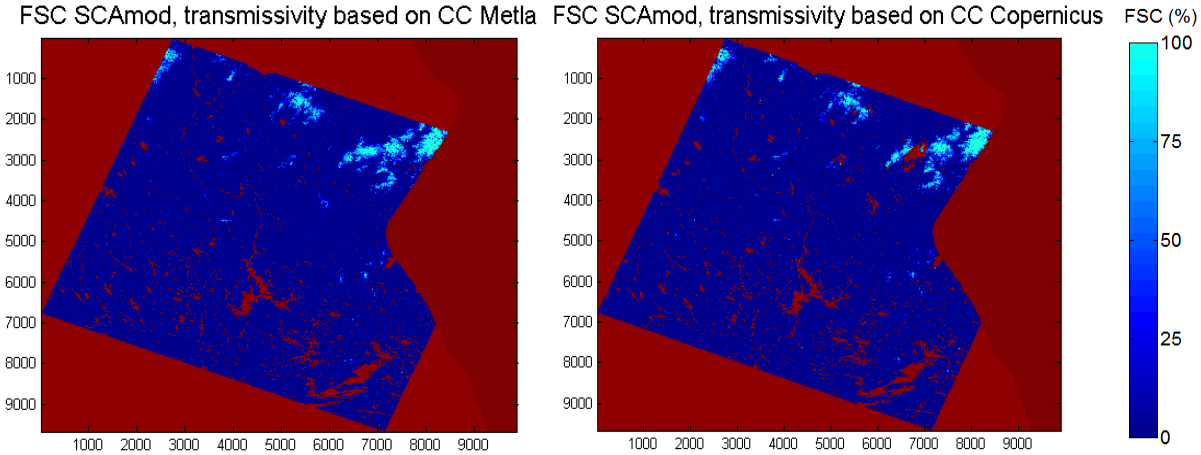

Figure 10.14: FSC maps for the LS-8 scene 190/13 of 17 May 2013. *Left:* SCAmod and Metla CC-derived transmissivity was applied; *Right:* SCAmod and Copernicus HRL CC data was applied. The red areas represent water or no-data (see that both CC datasets end at the Finnish-Russian borderline in the eastern side of the scenes).

These guidelines only describe the basic idea of using SCAmod and the transmissivity data for the provisions of high resolution FSC maps. It will be demonstrated later on how the approach works outside Finland when only Copernicus HRL CC and Maryland CC are available (the former is only for Europe, the latter covers the whole Northern Hemisphere. It is evident that the quality and representativeness of the CC-data plays a key role in the success of the FSC-estimation by means of SCAmod. On the other hand, for areas that do have a proper seasonal snow cover, it is very likely that the transmissivity can be generated also directly from reflectance acquisitions. This means that CC-derived transmissivity generation may serve only as a complementary data source. The option chosen depends also on the extent of the area of interest: generation of a 25 m transmissivity maps for the whole northern hemisphere would probably rely on the CC data due to otherwise too laborious work with high-resolution data, as it would comprise selection of full snow covered scenes, evaluation of feasible values for snow reflectance, cloud screening etc. For individual scenes this is not a problem of course.

11. REFERENCES

Bippus, G. (2011). Characteristics of summer snow areas on glaciers observed by means of Landsat data. *Doctoral Thesis*, pp. 231.

György Büttner. Guidelines for verification and enhancement of high-resolution layers produced under GMES initial operations (GIO) Land monitoring 2011 – 2013. Report, European Environment Agency, 2012

Cline, D., Rost, A., Painter, T., & Bovitz, C. (2010). NOAA - ATBD Snow Cover. *NOAA NESDIS Center for Satellite Applications and Research*, *2.1*, 1–40.

Documentation for the Shuttle Radar Topography Mission (SRTM) Water Body Data Files. (2005), 1–2.

Dozier, J., & Painter, T. H. (2004). Multispectral and Hyperspectral Remote Sensing of Alpine Snow Properties. *Annual Review of Earth and Planetary Sciences*, *32*(1), 465–494. doi:10.1146/annurev.earth.32.101802.120404

Ekstrand, S. (1996). Landsat TM-Based Forest Damage Assessment: Correction for Topographic Effects. *Photogrammetric Engineering and Remote Sensing*, *62*(2), 151–161.

Hall, D. K., Riggs, G. A., & Salomonson, V. V. (1995). Development of Methods for Mapping Global Snow Cover Using Moderate Resolution Imaging Spectroradiometer Data. *Remote Sensing of Environment*, *54*(2), 127–140.

Hansen, M. C., Potapov, P. V., Moore, R., Hancher, M., Turubanova, S. A., Tyukavina, A., … Townshend, J. . R. G. (2013). High-resolution global maps of 21st-century forest cover change. *Science (New York, N.Y.)*, *342*, 850–853. doi:10.1126/science.1244693

Klein, A. G., Hall, D. K., & Riggs, G. A. (1998). Improving snow cover mapping in forests through the use of a canopy reflectance model. *Hydrological Processes*, *12*, 1723–1744.

Metsämäki, S., Pulliainen, J., Salminen, M., Luojus, K., Wiesmann, A., Solberg, R., … Ripper, E. (2015). Introduction to GlobSnow Snow Extent products with considerations for accuracy assessment. *Remote Sensing of Environment*, *156*, 96–108. doi:10.1016/j.rse.2014.09.018

Nagler, T., Bippus, G., Heidinger, M., Malcher, P., Müller, F., Ripper, E., Rott, H., Sandner, R., and Voglmeier, K. (2012). ASAG – Preparation for a GMES Downstream Service for Snow and Glacier Monitoring in Alpine Regions. Final Report of the Project 819755 of the 6th call of ASAP, pp. 178.

Painter, T.H., J. Dozier, D.A. Roberts, R.E. Davis, R.O.Green. 2003. Retrieval of subpixel snow covered area and grain size from imaging spectrometer data. Reote Sensing of Environment. 85, 64-77.

Painter, T. H., Rittger, K., McKenzie, C., Slaughter, P., Davis, R. E., & Dozier, J. (2009). Retrieval of subpixel snow covered area, grain size, and albedo from MODIS. *Remote Sensing of Environment*, *113*(4), 868–879. doi:10.1016/j.rse.2009.01.001

Poon, S. K. M. (2004). *UCGE Reports Hydrological Modelling Using MODIS Data for Snow Covered Area in the Northern Boreal Forest of Manitoba by*. *Thesis*.

Poon, S. K. M., and Valeo, C. (2006). Investigation of the MODIS snow mapping algorithm during snowmelt in the northern boreal forest of Canada. *Canadian Journal of Remote Sensing*, *32*, 254–267.

Rosenthal, W., & Dozier, J. (1996). Automated Mapping of Montane Snow Cover at Subpixel Resolution from the Landsat Thematic Mapper. *Water Resources Research*, *32*(1), 115–130. doi:10.1029/95WR02718

Salomonson, V. ., & Appel, I. (2004). Estimating fractional snow cover from MODIS using the normalized difference snow index. *Remote Sensing of Environment*, *89*(3), 351–360. doi:10.1016/j.rse.2003.10.016

Salomonson, V. V., & Appel, I. (2006). Development of the Aqua MODIS NDSI fractional snow cover algorithm and validation results. *IEEE Transactions on Geoscience and Remote Sensing*, *44*(7), 1747–1756. doi:10.1109/TGRS.2006.876029

SRTM Water Body Data Product Specific Guidance. (2003), *v2.0*, 1–4.

Tomppo, E. "The Finnish multi-source National Forest Inventory - small area estimation and map production." In: Kangas, A. & Maltamo, M. (eds.). Forest inventory. Methodology and applications. Managing Forest Ecosystems. Vol 10. Springer, Dordrecht. p. 195-224, 2006.

USGS Landsat Missions: http://landsat.usgs.gov/index.php (accessed 31 March 2016)

USGS Landsat &Sentinel http://landsat.gsfc.nasa.gov/?p=10643 (accessed 31 March 2016)